

LOCKHEED MARTIN ENERGY RESEARCH LIBRARIES



3 4456 0515900 2

CENTRAL RESEARCH LIBRARY
DOCUMENT COLLECTION

2

ORNL-3960
UC-4 - Chemistry

DATA COLLECTION AND EVALUATION WITH
AN X-RAY DIFFRACTOMETER DESIGNED FOR
THE STUDY OF LIQUID STRUCTURE

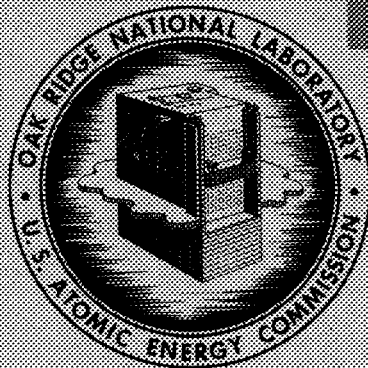
H. A. Levy
M. D. Danford
A. H. Narten

CENTRAL RESEARCH LIBRARY
DOCUMENT COLLECTION

LIBRARY LOAN COPY

DO NOT TRANSFER TO ANOTHER PERSON

If you wish someone else to see this
document, send in name with document
and the library will arrange a loan.



OAK RIDGE NATIONAL LABORATORY

operated by

UNION CARBIDE CORPORATION

for the

U.S. ATOMIC ENERGY COMMISSION

Printed in USA. Price \$3.00. Available from the Clearinghouse for Federal
Scientific and Technical Information, National Bureau of Standards,
U.S. Department of Commerce, Springfield, Virginia 22151.

LEGAL NOTICE

This report was prepared as an account of Government sponsored work. Neither the United States, nor the Commission, nor any person acting on behalf of the Commission:

- A. Makes any warranty or representation, expressed or implied, with respect to the accuracy, completeness, or usefulness of the information contained in this report, or that the use of any information, apparatus, method, or process disclosed in this report may not infringe privately owned rights; or
- B. Assumes any liabilities with respect to the use of, or for damages resulting from the use of any information, apparatus, method, or process disclosed in this report.

As used in the above, "person acting on behalf of the Commission" includes any employee or contractor of the Commission, or employee of such contractor, to the extent that such employee or contractor of the Commission, or employee of such contractor prepares, disseminates, or provides access to, any information pursuant to his employment or contract with the Commission, or his employment with such contractor.

ORNL-3960

Contract No. W-7405-eng-26

CHEMISTRY DIVISION

DATA COLLECTION AND EVALUATION WITH AN X-RAY DIFFRACTOMETER
DESIGNED FOR THE STUDY OF LIQUID STRUCTURE

H. A. Levy, M. D. Danford, and A. H. Narten

JULY 1966

OAK RIDGE NATIONAL LABORATORY
Oak Ridge, Tennessee
operated by
UNION CARBIDE CORPORATION
for the
U.S. ATOMIC ENERGY COMMISSION

LOCKHEED MARTIN ENERGY RESEARCH LIBRARIES



3 4456 0515900 2

CONTENTS

ABSTRACT	v
ACKNOWLEDGEMENTS	vii
1. INTRODUCTION	1
2. DESCRIPTION OF DIFFRACTOMETER	1
2.1 General Design	1
2.2 Mechanical System	3
2.3 Monochromator	7
2.4 Slit System	10
2.5 Detector and Electronic System	13
2.6 Sample Mount and Furnace	14
3. ADJUSTMENT OF DIFFRACTOMETER	15
3.1 Mechanical and Slit System	15
3.2 Monochromator	18
3.3 Sample Position	18
4. COLLECTION OF DATA	19
5. THE DIFFRACTION OF X-RAYS BY LIQUIDS	20
5.1 Debye's Equation for the Total Intensity	20
5.2 Reduced Intensity and Radial Distribution Function	24
6. PROCESSING OF DATA	27
6.1 The Raw Data	27
6.2 Background	27
6.3 Polarization	29
6.4 Absorption	29
6.5 Compton Scattering	29
6.6 Normalization	33

6.7	Reduced Intensity and Radial Distribution Function	33
7.	INTERPRETATION OF DATA	39
7.1	Simple Liquids	39
7.2	Complex Liquids	41
7.3	Solutions	46
8.	APPENDIX	48
8.1	Absorption Corrections for a Flat Sample	48
8.1.1	Highly Absorbing Samples	48
8.1.2	Deeply Penetrated Samples	52
8.2	Focussing Condition for Crystal Monochromator	54
9.	REFERENCES	54

ABSTRACT

An x-ray diffractometer designed specifically for studies of structure in liquids is described in detail. The diffraction pattern from the horizontal surface of the liquid sample is obtained with a divergent beam technique similar to the Bragg-Brentano flat sample system used for powder samples. The instrument provides for simultaneous angular motion of the x-ray tube and the detector about a horizontal axis lying in the liquid surface. This method eliminates sample holder absorption and scattering. A small furnace for high temperature work is included in the design. Monochromatic x-radiation, essential to good work with liquids, is obtained through the use of a bent and ground crystal monochromator mounted in the diffracted beam.

Data collection with this instrument, and the various correction procedures applied to the raw data are discussed in detail. The theory of x-ray diffraction by liquid systems is reviewed in the light of recent developments in this field. The derivation of reduced intensity and radial distribution functions from the diffraction data is described, and ways of obtaining meaningful information on liquid systems from these functions are outlined.

ACKNOWLEDGEMENTS

Design and construction of the x-ray diffractometer described in this report was begun in 1954 under the direction of H. A. Levy of the ORNL Chemistry Division. Operation of the machine began in the spring of 1955, with development continued to the present time.

Initial work was supervised by P. C. Sharrah, on leave from the University of Arkansas for one year, assisted by M. D. Danford who was in charge of the instrument until 1964. A great deal of the design and supervision of construction are credited to D. L. Holcomb of the Plant and Equipment Division. Later major contributors were P. A. Agron, who was with the project for several years, O. E. Esvai, ORINS fellow during 1962, and A. H. Narten, who joined the project in 1964.

Important contributions in the indicated fields are due to:

Instrument Design:

L. H. Chase, J. K. East, R. D. Ellison, E. Fairstein, J. F. Potts, R. B. Splittgerber, H. N. Wilson.

Spectrometer Fabrication:

B. Cook, D. Holt, J. E. Lacey, M. E. Smith, N. C. Wilkins, C. W. Wright.

Optical System:

E. S. Cantrell, N. C. Carothers, V. E. Walker, N. E. Wilkins.

Instrument Maintenance:

E. A. Davis, J. H. Day, J. Eddlemon, L. D. Hunt, M. Naegel, R. B. Splittgerber.

Special Welding and Brazing:

J. W. Hunley, J. J. Prisliger, C. E. Shubert.

1. INTRODUCTION

The x-ray diffraction patterns produced by liquids can be studied to gain information about the spatial distribution of atoms within the liquid under study. The formal approach to this problem was introduced and developed by Zernicke and Prins¹ and Debye and Menke².

Excellent reviews are available on the experimental methods which are currently used,³ on fundamental aspects of interpreting the experimental data,³ on the sources of errors³, and on the results obtained up to 1960.⁴

2. DESCRIPTION OF DIFFRACTOMETER

2.1 General Design

The apparatus described here⁵ is designed to obtain diffraction patterns from the free surface of a liquid by the use of counting techniques. The Bragg-Brentano focussing arrangement⁶ commonly used in powder spectrometers is applied. Fig. 1 shows schematically the arrangement of the x-ray tube X, sample HH, and the detector arm with monochromator M and detector D, and Fig. 2 shows the physical arrangement. The arm containing the Mo target x-ray tube and the arm containing the monochromator and detector are caused to rotate at the same angular rate and in opposite sense about a horizontal axis A (Fig. 1) lying on the surface HH of the liquid. The slits S_1 , S_2 and S_3 serve to define the incident and scattered beams and to determine their divergence δ . This arrangement, with the mean angle α between the incident beam and the sample surface always equal to the mean angle β between the scattered ray and the sample surface, makes possible the use of a divergent beam. This geometry causes any ray drawn from X to the sample surface HH, and thence to S_3 , to have experienced the same scattering angle at the surface of the sample to an approximation present only because

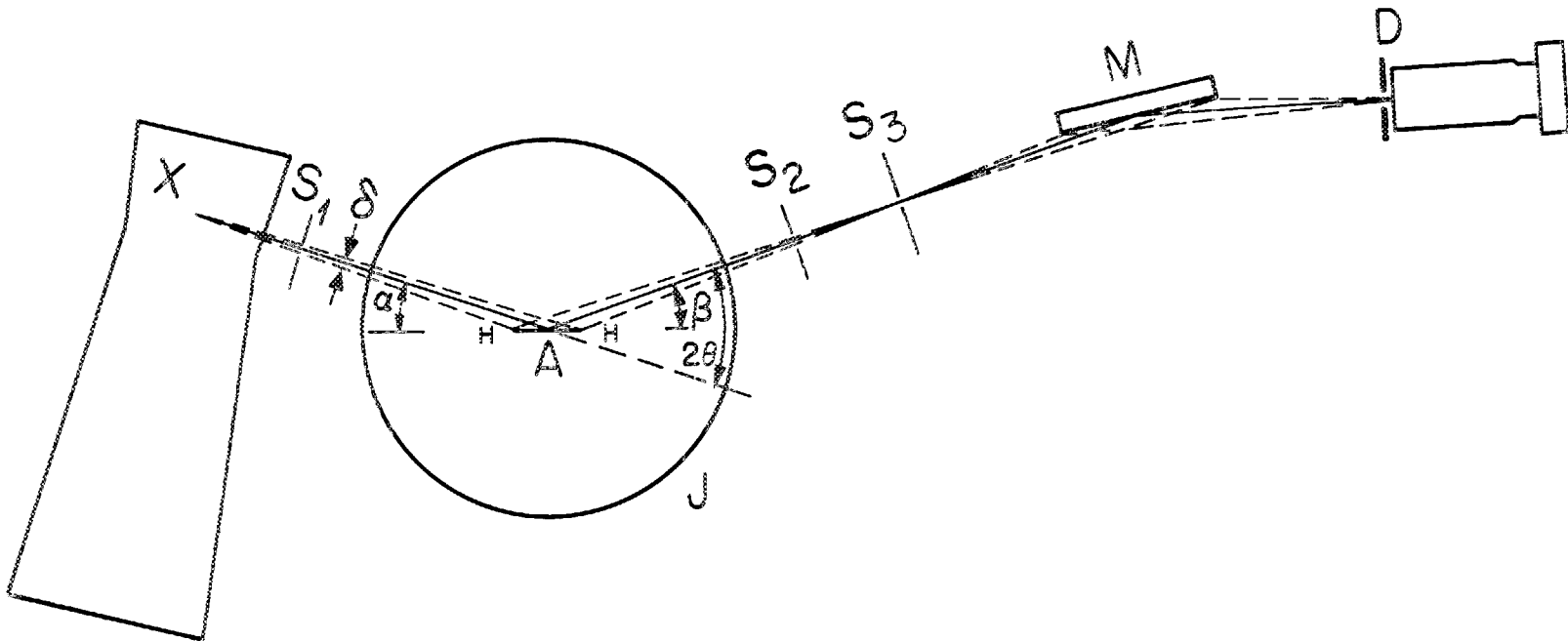


Fig. 1. Instrument Geometry.

the sample represents the chord of the circle containing points X, A and S_3 rather than an arc, and because of the finite size of the source X and receiving slit S_3 . The divergent beam method considerably increases the intensity of the scattered beam over that expected from a finely collimated beam. The condition that the angles α and β are always equal results in an absorption correction which (for a highly absorbing sample) is constant with angle (see section 8.1), and thus to that extent simplifies the treatment of the data. The crystal monochromator M is of the focussing type⁷ and is set to reflect the characteristic $K\alpha$ radiation of the source; it consists of a sodium chloride crystal bent to a chosen radius and then ground to half that radius, so that the final arc conforms theoretically to the circle determined by the three points S_3 , the point at the center of the face of the monochromator M, and a point in the sensitive portion of the detector D. The detector D set to receive the final beam as reflected by the monochromatizing crystal consists of a sodium iodide (Tl activated) scintillation crystal and a photomultiplier tube in conjunction with a linear amplifier and a differential discriminator.

2.2 Mechanical System

The arm for moving the x-ray tube and the arm for moving the detector and monochromator are clearly visible in Fig. 2. The rotation of these two arms about a horizontal axis is made possible by their being mounted on two carefully aligned heavy bearings which consist of standard rotary tables for milling machines*.

The drive consists of a three-speed synchronous motor and a gear train providing suitable reduction in speed. The three speeds of the motor, along

*Troyke Manufacturing Company, Cincinnati, Ohio.

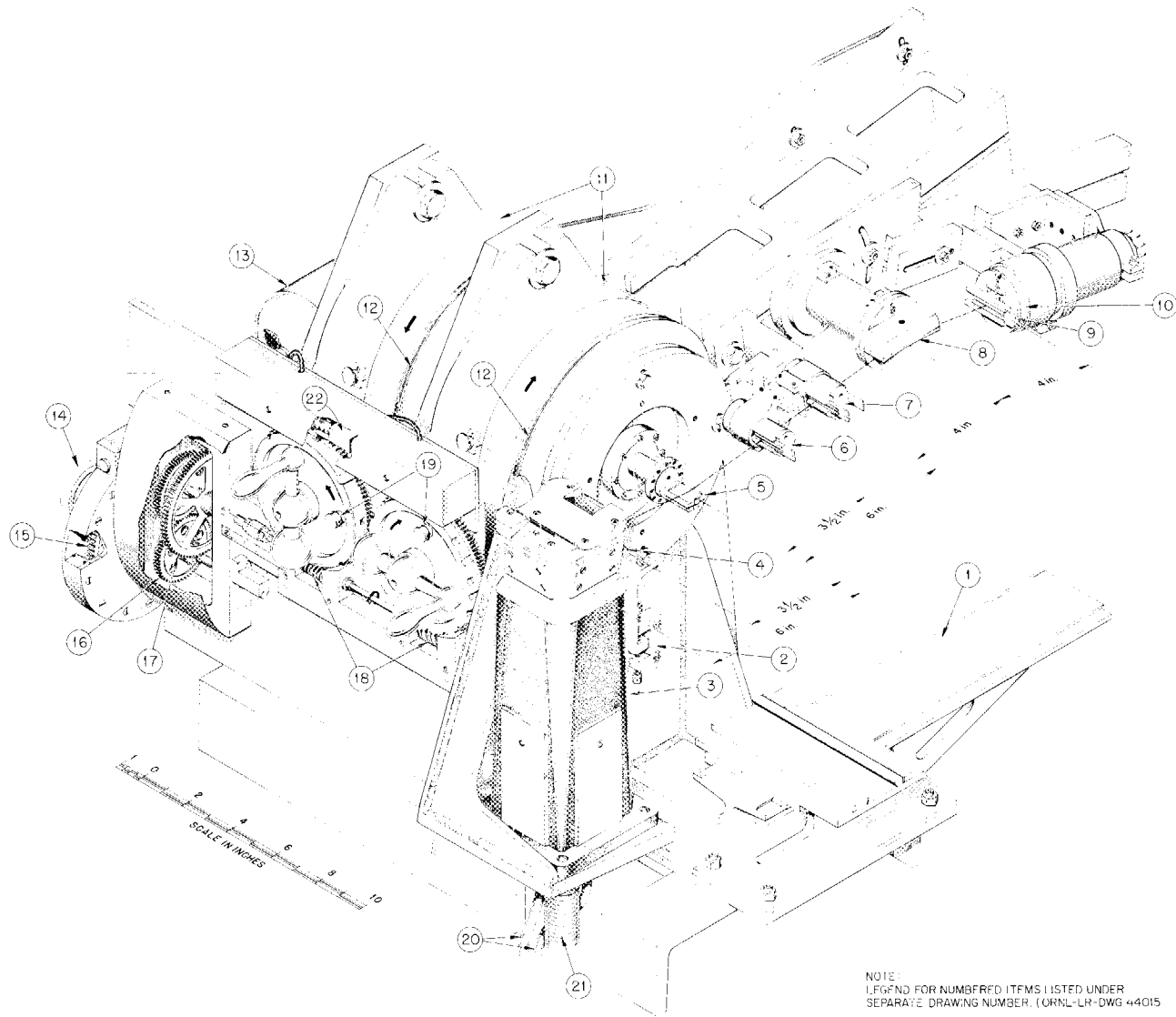


Fig. 2. X-Ray Diffractometer for Liquids.

X-RAY DIFFRACTOMETER FOR LIQUIDS*

1. OPTICAL BENCH TO MOUNT ALIGNING MICROSCOPE.
2. SAMPLE HEIGHT ADJUSTMENT.
3. NORELCO X-RAY TUBE AND HOUSING.
4. NORELCO DIVERGENCE SLIT ASSEMBLY.
5. SAMPLE TRAY AND MOUNTING.
6. NORELCO DIVERGENCE SLIT ASSEMBLY (USED AS SCATTER SLIT).
7. NORELCO RECEIVING SLIT ASSEMBLY.
8. BENT AND GROUND NaCl CRYSTAL.
9. BAFFLE SLIT FOR DETECTOR.
10. NaI(Tl) SCINTILLATION CRYSTAL AND PHOTOMULTIPLIER TUBE (TYPE DUMONT 6291).
11. NINE-IN. ROTARY TABLES (TROYKE MODEL BH-9), GEAR RATIO 90:1.
12. CABLES SUPPORTING COUNTERWEIGHTS RIDE IN GROOVES.
13. 3-SPEED SYNCHRONOUS MOTOR (900-1800-3600 RPM).
14. GEAR CHANGE KNOW (IN AND OUT, GEAR RATIO SETTING).
15. 120-TOOTH WORM GEAR AND WORM.
16. 54:54-TOOTH SPUR GEAR PAIR.
17. 12:96-TOOTH SPUR GEAR PAIR.
18. 120-TOOTH WORM GEAR AND WORM.
19. PINS DISENGAGE GEARS FROM SHAFT FOR MANUAL SETTING.
20. WATER TUBES.
21. HIGH VOLTAGE CABLE.
22. MICROSWITCH (3 OTHERS FOR ALTERNATE CHOICE OF CAMS).

*LEGEND COMPOSED FOR ORNL-LR-DWG. 43071.

with two settings on the gear train, give a total of six angular driving rates of the arms extending from 1° to $1/32^\circ$ per minute of half-scattering angle θ (Fig. 1) as summarized in Table 1. The two arms can be operated

Table 1.

Scanning Rates (deg/min) of the Half-Scattering Angle θ

Motor RPM	Gear	
	Low	High
900	$1/32$	$1/4$
1800	$1/16$	$1/2$
3600	$1/8$	1

manually by the two cranks visible in Fig. 2 after releasing the crank shafts from the two driving gears with the pins provided. The worm gear drive is such that one revolution of the crank rotates the table with its arms through an angle of 4° . Verniers serve to determine accurately the angular settings of the two arms; but scales mounted and the drive gears on the crank arms can be used more conveniently to determine this angle to within 2 minutes of an arc, if the backlash in the worm gear drive has been taken up. Microswitches and cams on one of the drive gears (Fig. 2) make possible the use of step-scanning for collecting intensity data. Safety limit switches in the electrical circuit are provided to stop the motor at the extreme positions of the arms.

The tracks for the various components on the monochromator and detector arm were fabricated from magnesium in order to reduce weight. Both arms are counterbalanced by lead weights on arms below the table which

are interconnected by cables. A counter weight on the detector arm serves to reduce torsional effects as the detector arm rotates.

The x-ray tube with housing is standard equipment^{*} and is powered by a constant potential from a diffraction unit.^{**}

2.3 Monochromator

The crystal monochromator is of the focussing type and consists of a thin slab of synthetically crystallized sodium chloride approximately 1"x2-1/2"x1/8" bent to a chosen radius (80.4 cm), ground to one-half the radius (40.2 cm), and set to reflect from (200) planes. Fig. 3 shows some of the conditions which must be satisfied by the focussing crystal. The symbols S_3 , M and D designate the receiving slit, monochromator, and detector, as shown in Fig. 1, and L' is the distance from the slit to the center of the monochromator, and also from the center of the monochromator to the point at which it is desired to detect the scattered x-rays. When the crystal is bent and ground as described, its (200) planes will be tangent to the circle at the center of the monochromator, C, and will touch the circle at all other points such that the plane normals will all point towards E and bisect arc S_3ED . This is the condition for Bragg reflection (see section 8.2). The equation

$$R = L'd/\lambda \quad (2.3.1)$$

is obtained by substituting the expression for $\sin \theta$ obtained from triangle S_3CE in Fig. 3 in Bragg's law, d being the interplanar distance of the monochromator crystal. For the rock salt crystal set for plane (200) to reflect $\text{MoK}\alpha$ radiation, equation 2.3.1 yields $R = 40.2$ cm, with an assumed

*North American Phillips

**General Electric XRD-3.

ORNL-LR-DWG. 13824 A

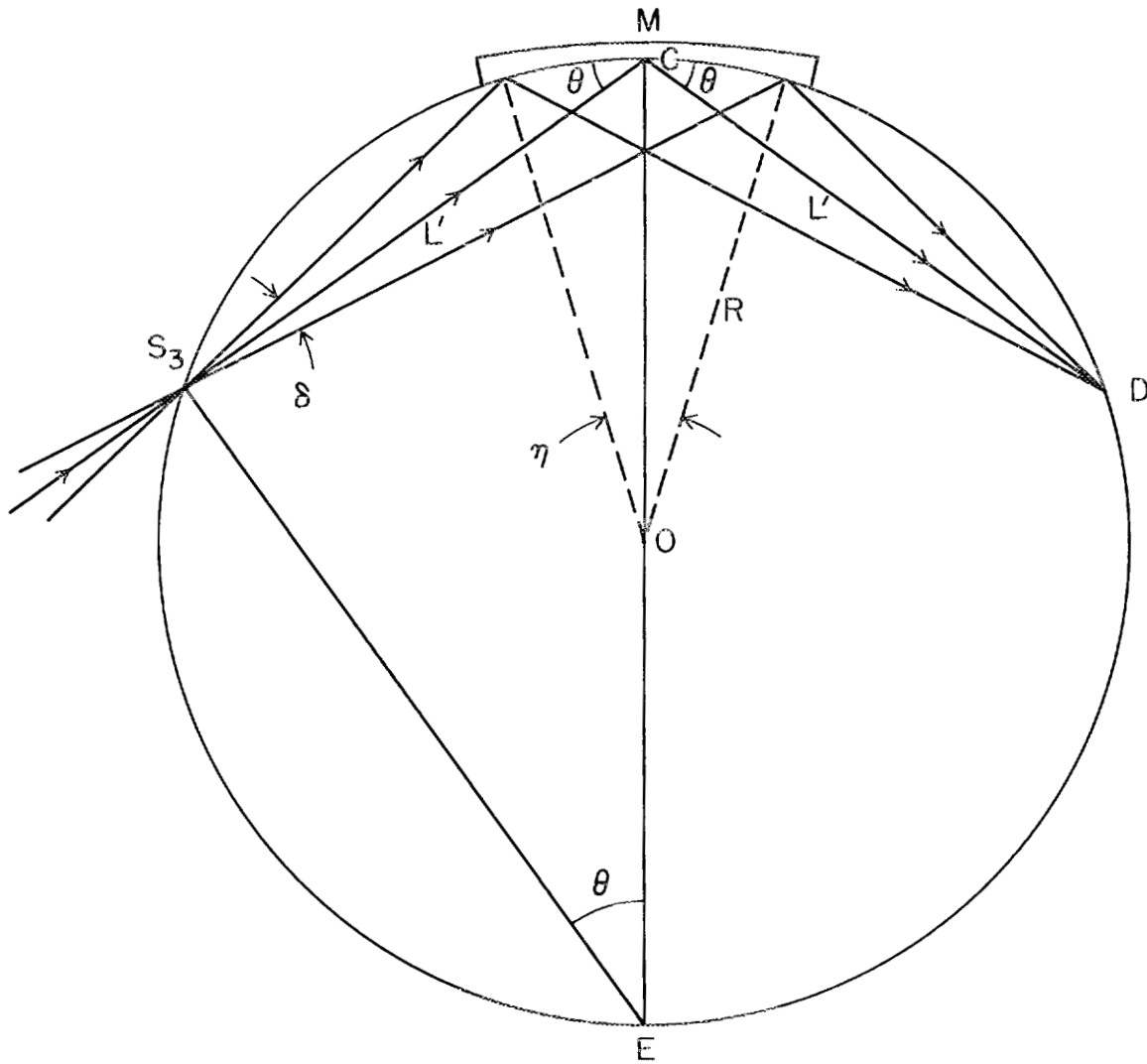


Fig. 3. Crystal Monochromator Geometry.

design value of 4" for L' . This value of L' was adopted as reasonable, and provision was made to grind the crystal to an ultimate radius of 40.2 cm.

The geometry of Fig. 3 shows that the angular dimension η of the crystal needed to accept all radiation from S_3 , if the divergence is σ , is given by

$$\eta = 2\sigma \quad (2.3.2)$$

and the length S of the crystal needed will be

$$S = R\eta = 2R\sigma \quad (2.3.3)$$

The largest beam divergence used is 4° and this value substituted in equation 2.3.3 along with an R of 40.2 cm gives a required crystal size of 5.6 cm, well within the 2.5" size crystals adopted. Beams of smaller divergence use proportionally smaller amounts of crystal surface and should be less sensitive to imperfections in the focussing system.

Convex steel templates of 80.4 cm and 40.2 cm radius were made for use in grinding and bending the crystal, while concave steel templates of 80.4 cm radius were made for mounting purposes. A small universal grinding machine was adapted for the precision grinding of these templates by a method outlined by DuMond⁸. The templates obtained were checked for accuracy by measurements made with an instrument maker's microscope. The flat crystal slabs were bent plastically to conform fairly well to the 80.4 cm convex template by applying pressure gradually to the crystal through a tennis ball with a drill-press clamping vise⁹. The plastic bending was aided by covering the crystal with a saturated salt solution, which was dropped onto the crystal every few minutes with an eye dropper. The crystal was then secured by means of a polymerizing glue to a concave mount of 80.4 cm. radius. The face of the bent crystal was the ground with the convex template of 40.2 cm radius. Alundum grinding powder suspended in kerosene served as the grinding abrasive.

This method produced small scratches and irregularities which were removed by lapping the crystal briefly with a cylindrical lapping template. After the monochromator had been in operation for a few weeks a sizable reduction in its reflected intensity was noted. Relapping of its surface restored the intensity, and the surface of the crystal was sprayed with a thin film of an acrylic base plastic^{*} to protect it from moisture.

2.4 Slit System

The horizontal slit S_1 (Fig. 1) with its verticle Soller slit system is mounted on the face of the x-ray tube housing and arranged so that a slight vertical motion of the slit is produced by rotating the assembly. This slight vertical motion of the slit S_1 makes it possible to direct the beam from the focal spot of the x-ray tube directly toward the axis A of the instrument where the sample surface is located. The system containing a set of vertical Soller slits and the horizontal slits S_2 and S_3 is attached to the arm supporting the monochromator and the detector and provides for independent adjustment of each by an arrangement similar to that provided for S_1 (Fig. 2). The other major mechanical adjustment provides for a small rotation of the assembly consisting of the slotted tracks for holding the slits S_2 and S_3 and the monochromator and detector. This assembly is secured to the main arm by screws through slots which permit accurate rotation through approximately 4° about a small bearing secured to the main axis of the instrument. A baffle slit directly in front of the detector (Fig. 2) serves to reduce background radiation.

The slit arrangement currently used (Fig. 1 and 2) is different from the usual arrangement, and was chosen because it defines the x-ray beam so

* Krylon, Inc., 2601 North Broad St., Philadelphia 32, Pennsylvania.

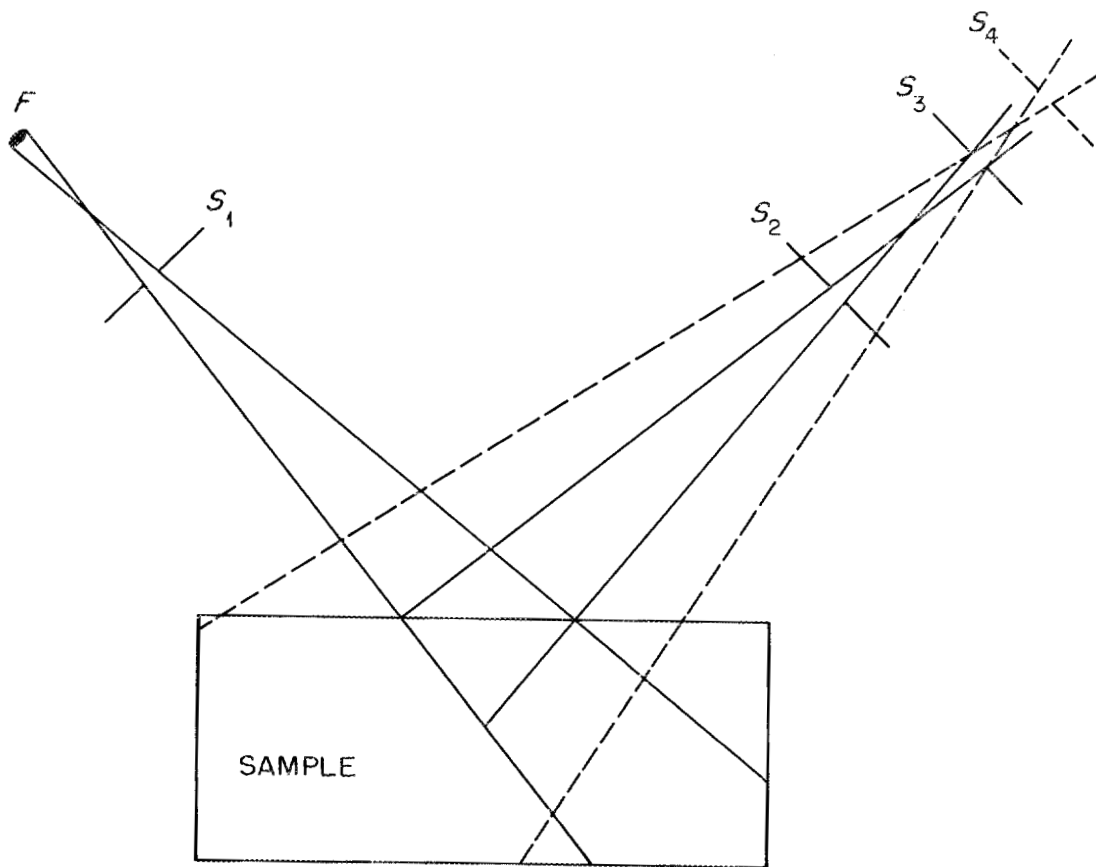


Fig. 4. Geometry of the Slit Arrangement.

that appropriate corrections for sample penetration can be applied (see section 8.1). The absorption correction for the Bragg-Brentano para-focussing arrangement is independent of scattering angle provided all scattered radiation leaving the sample and passed by the receiving slit reaches the detector. Consequently, when the sensitive angle of the detector is limited by the insertion of a scatter slit, care must be taken that this slit is sufficiently large. When the depth of penetration of the radiation into the interior of the sample is small, a scatter slit defining an angle a few per cent larger than that defined by the divergence slit is satisfactory. It may not be widely appreciated, however, that cases can arise in which more than a nominal enlargement is necessary; with samples having low absorption coefficients, the required scatter slit may become inconveniently large, especially at small scattering angles, and may allow passage of excessive stray radiation. The use of too small a scatter slit will manifest itself, as has been observed at this laboratory, in an angularly dependent normalization constant (see section 6.6) between patterns measured with different divergence slits.

Fig. 4 shows the geometry of the slit arrangement. In contrast to the usual arrangement, the sensitive angle of the detector is carefully limited by a scatter slit S_2 to "see" exactly the same area of the sample surface as is illuminated by the primary beam. In order to achieve this condition with finite-sized effective source and receiving slit, the scatter slit is moved from its usual location between the receiving slit and detector (dashed line S_4 in Fig. 4) to a location between the receiving slit and the sample. The divergence slit S_1 and the scatter slit S_2 are made equal in size and are placed equi-distant to the spectrometer axis. The slit S_3 is approximately the size of the focal spot F of the x-ray tube and symmetric to it.

This arrangement possesses some corollary advantages. The background of stray radiation is reduced, particularly at small angles. The lower limit of scattering angle which may be reached with a given slit pair and given sample size is extended. Resolution from the primary beam at very small scattering angles is materially augmented, particularly if an additional baffle slit is added in the location S_{11} usually occupied by the scatter slit. The depth of sample required may sometimes be materially reduced.

2.5 Detector and Electronic System

Detection of the diffracted beam is by means of a scintillation counter in conjunction with a linear amplifier, a pulse height single-channel analyzer and a count scaler-timer. A ratemeter and recording potentiometer provide an alternate method of recording the data.

The detector is a sodium iodide (thallium activated) crystal approximately $1/32$ " thick, $1/8$ " wide and $5/8$ " long, held in place on a DuMont 6291 photomultiplier tube by a light-tight can. The photon counting efficiency was aided by placing silicone grease between the crystal and the photomultiplier, and by using an aluminum foil reflector. A beryllium window admits the x-rays to the crystal. The photomultiplier is currently operated at about 110 volts per stage.

The amplified pulses produced when $\text{MoK}\alpha$ radiation is reflected by the (111) planes of nickel powder give a fairly broad pulse-height distribution centered at 16.5 volts and extending sensibly from 12 to 23 volts. A window of 1 volt was used in obtaining this result. Based on this information, the window and discriminator are set for use such that pulses from 10.5 to 20.5 volts will be detected. This effectively rejects any pulses which might arise from the second order half-wavelength radiation from the continuous spectrum, reflected by the monochromator.

Measurements with $\text{AgK}\alpha$ x-rays (Cd-109 source), $\text{MnK}\alpha$ x-rays (Fe-55 source), and $\text{MoK}\alpha$ x-rays gave pulse height curves whose maxima are closely proportional to the energy. The Cd-109 and Fe-55 sources are placed directly in front of the window of the scintillation detector for these measurements. They are useful as a check on the performance of the electronic system because this can be done conveniently at any time during the long runs required for data collection.

2.6 Sample Mount and Furnace

The sample, which may be contained in a flat tray (Fig. 2), is located on a stainless steel shelf supported by a stainless steel tube attached to the main base. The steel tube was reduced to a wall thickness of 0.010" so that the sample and its supporting shelf can be heated to red heat without a great loss by conduction along the supporting tube. The thermocouples are inserted in holes provided in the shelf through a kovar seal. A small stainless steel tube with an outside diameter of 0.035" also passes through this seal. This makes it possible to evacuate the sample region and to introduce an inert gas when a beryllium cup is bolted against the flange of the sample shelf. Both stainless steel and molybdenum delta-ring gaskets have been used successfully to seal the beryllium cup (0.012" wall) containing the sample region from the main furnace. The beryllium cup is heated by nichrome V wire wound on an accurately fabricated ceramic cylinder located on its outside. One or more stainless steel cylinders around the beryllium cup serve as heat radiation shields. The whole furnace region is surrounded by a water-cooled jacket which can be evacuated to pressures below one micron in order to reduce heat losses by conduction to a minimum. It has a slot for passage of the x-ray beam which is covered with a 0.012" beryllium strip with its inner surface polished so that a vacuum tight seal is obtained when the strip is

clamped against a neoprene o-ring gasket. The inner radiation shields have similar slots for passage of the x-ray beam. A liquid nitrogen trap and vacuum exhaust to a filtered hood system provide safeguard against the danger of beryllium oxide or other compounds being freed into the room if there should be a failure of the vacuum system while the furnace is hot. As an indication of the degree of success which has been reached with the radiation shielding and evacuated furnace, a power of approximately 85 watts is adequate to maintain a temperature of 650°C.

The complete furnace with the sample shelf can be raised or lowered and leveled to place the sample surface in the proper position by two adjusting screws (Fig. 2).

3. ADJUSTMENT OF DIFFRACTOMETER

3.1 Mechanical and Slit Systems

The initial mechanical adjustments may be carried out in the following manner after the main x-ray table has been approximately levelled:

- (1) The slit S_1 is approximately adjusted until the x-ray beam falls symmetrically on the instrument axis, as determined by a fluorescent screen.
- (2) The fluorescent screen is removed, and a very fine wire (0.01" diameter) supported by a yoke attached to a goniometer is placed in position. This is accomplished by securing the goniometer to a bar which fits tightly through the center of the rotary milling machine heads (Fig. 2).
- (3) The wire is adjusted through use of the goniometer mount so that it is parallel to the spectrometer axis, and centered so that a 180° rotation of the wire produces no vertical motion at either end. These adjustments are made using a traveling microscope; observations of adjustments at right angles to the viewer are made possible by an objective prism mounted at the end of the microscope, the base for which is shown in Fig. 2.

(4) The mounting track which holds the S_2S_3 slit assembly and the monochromator is rotated slightly upward or downward using an adjusting screw until it is level as determined by a good quality level.

(5) Slits S_2 and S_3 can be made to fall on the horizontal line S_1A (Fig. 1) either by small rotations of the component supporting each, or by vertical motion of their supports. The microscope is used to determine when the proper adjustment is reached.

(6) The beam is then adjusted to secure proper alignment of the x-ray tube focal spot, the slits, and the spectrometer axis. The primary beam is first scanned with only the detector arm in motion; slit S_1 is adjusted (by turning the slit or moving its support vertically) until the recorded intensity is split symmetrically by the fine wire in the spectrometer axis. Then, with both arms in motion, the beam is again scanned; source X, slit S_1 , axis A and slits S_2 and S_3 are considered aligned when, under these conditions, the recorded beam intensity is split symmetrically by the wire. If the now straight line $XS_1AS_2S_3$ is not horizontal (as determined by the traveling microscope), the source and detector arms as a whole are adjusted until the wire in the axis splits the recorded intensity of the primary beam in half at zero angle.

(7) A final check on the adjustments is made by scanning a complete diffraction pattern of a powdered material. That the reflections are properly received can be determined by testing with a detector directly behind the S_2S_3 slit system, or with the monochromator system in position. Fig. 5 shows typical results of these checks; here I is the integrated intensity of a Bragg reflection, F the atomic form factor, θ the half-scattering angle, and λ the wavelength of the x-radiation.

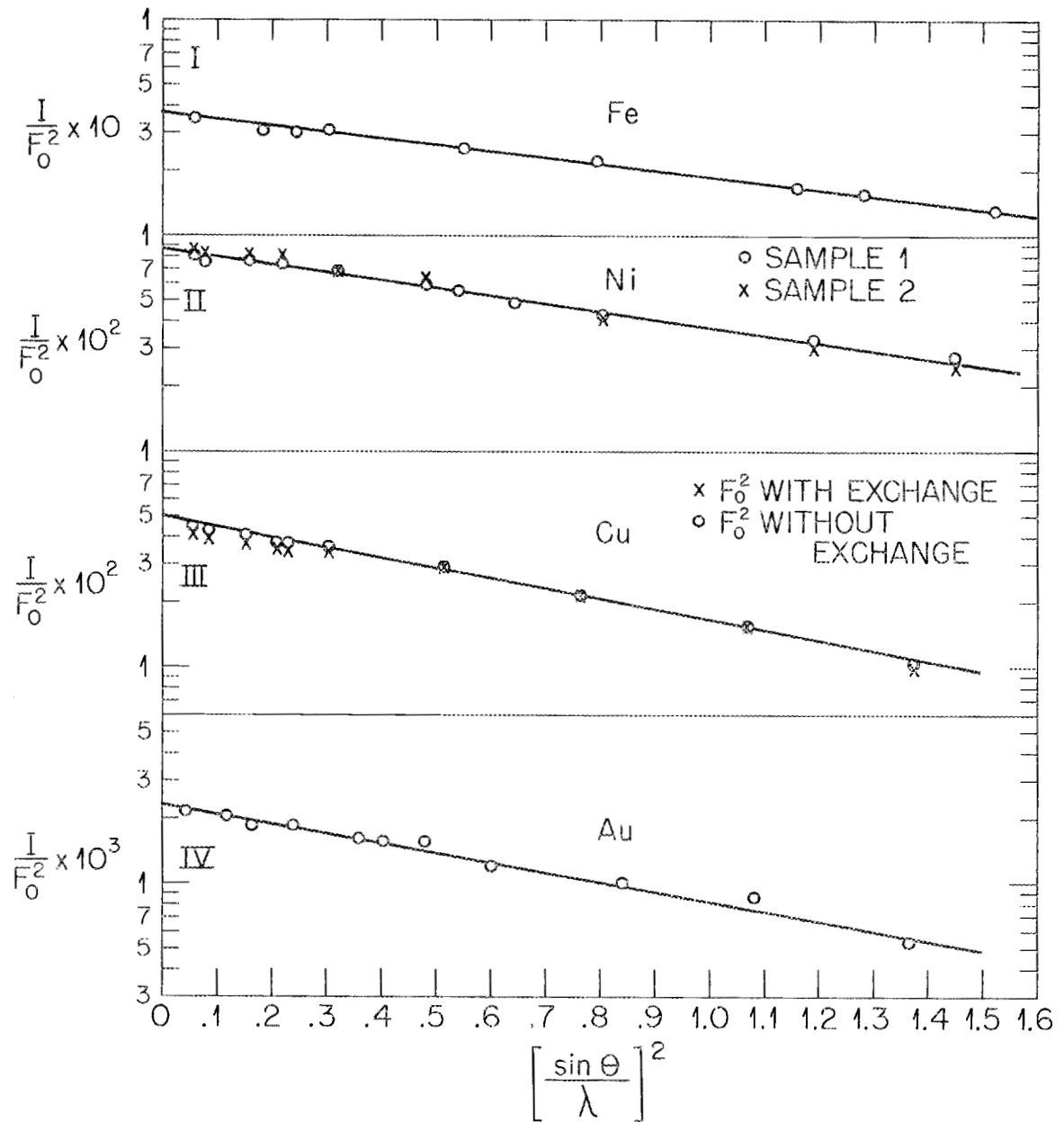


Fig. 5. Test of Instrument Alignment with Powdered Samples.

3.2 Monochromator

The monochromator must be set so that the basic condition for satisfying Bragg's law is fulfilled, and also must be placed to take advantage of the focussing for which the crystal was bent and ground. The first condition is satisfied by rotating the crystal slightly by tangent screws after being set at approximately the right angle. The second condition is obtained by placing the crystal at the proper distance from the slit S_3 which was designed to be 4". A distance slightly greater was found to give the most intense monochromatic beam.

With the crystal set at one distance from the slit S_3 and the detector set at twice the Bragg angle, the reflection is not difficult to find by turning the crystal slowly while operating the x-ray unit and the detecting equipment. A strong diffracted beam for this adjustment is obtained by setting on a strong reflection from powdered nickel.

3.3 Sample Position

If all the mechanical adjustments have been carried out properly, the x-ray beam as defined by the slits, x-ray tube, and monochromator system will be horizontal across the center A of the instrument axis (Fig. 1), when the arms are at their zero positions.

The final adjustment when a sample is placed in the instrument is to see that its surface is horizontal and at the proper height to have its surface lying on the axis A, which is brought about through the height adjustment (Fig. 2) on the sample assembly. It is necessary that the shelf which supports the sample be level if powder samples are to be used in the instrument, but any slight deviations from level will cause no difficulty with liquid samples. Even with molten liquids, the proper sample height can be established by using the x-ray detector to determine when the main beam is

being blocked by an amount previously established by tests with samples which can be handled at room temperature, such as powdered nickel and liquid mercury.

An alternate indicator for proper height of the sample consists in adjusting the height to maximize the detected beam when set on or near a known peak in the diffraction pattern.

4. COLLECTION OF DATA

Data collection from a liquid sample is usually restricted to a range from 4° to about 65° in θ , the half-scattering angle.

Below 4° , very small divergence slits must be used to define the main beam, and the sample must be of considerable length. The small slits imply very long counting times for accurate measurements. On the other hand, the accuracy obtainable with this instrument at very low angles is extremely sensitive to the instrument alignment, to curvature of the sample surface, and to the absorption correction (which shows a very pronounced angular dependence in this region; see section 8.1.2). These factors make the collection of data at very low angles somewhat unreliable.

At high angles, the scattered intensity becomes very weak because of the nature of the x-ray scattering function. Beam divergence is limited to 4° by the size of the monochromator. High angle data are essential for the high resolution obtainable with this instrument. Their benefit must be balanced against counting time. Extension of data collection beyond 65° in half-scattering angle would be necessary only for the determination of mean square amplitudes of interatomic distances in discrete molecules; this might be desirable in order to obtain quantitative information on the vibration frequencies of discrete molecules in the liquid state (see section 7.2).

The measured intensities are recorded either as the time necessary to achieve a fixed number of accumulated counts, or as the accumulated counts

for a preset time, at a given scattering angle. The data are taken in sections which cover a certain portion of the total angular range. Each of the sections is characterized by an initial angle, an increment by which the scattering angle is advanced, and the dimensions of the appropriate divergence and receiving slits. The initial angle is chosen so that it overlaps the preceding section. The angular increments range from 2 minutes of an arc for the lowest sections, to 1° for the highest section. The slits are chosen so that proper beam divergence for each section can be maintained. Several runs are made over each section until the accumulated counts reach a certain value, typically 100,000 to 500,000 for the low and high angle regions, respectively. It is necessary to accumulate such a large number of counts in order to safeguard reliability and high resolution for the structural information derived from the diffraction data. The accumulated counts for each section are chosen so that the statistical error in the reduced intensity function (see section 6.7) is held approximately uniform over the whole range of data.

At the beginning of each run over a section, the alignment of the sample surface in the instrument axis is carefully checked (see section 3.3). Sample temperature and pressure are recorded, and the electronic equipment is checked at close intervals (see section 2.5).

In extreme cases, data collection alone may take up to two months' time of continuous operation of the instrument.

5. THE DIFFRACTION OF X-RAYS BY LIQUIDS

5.1 Debye's Equation for the Total Intensity

Consider initially that an incident beam of x-radiation is directed upon an electron at point O (Fig. 6). Then the amplitude of radiation E_p scattered to point P, which is at a large distance R from O, is

ORNL-LR-DWG. 72794

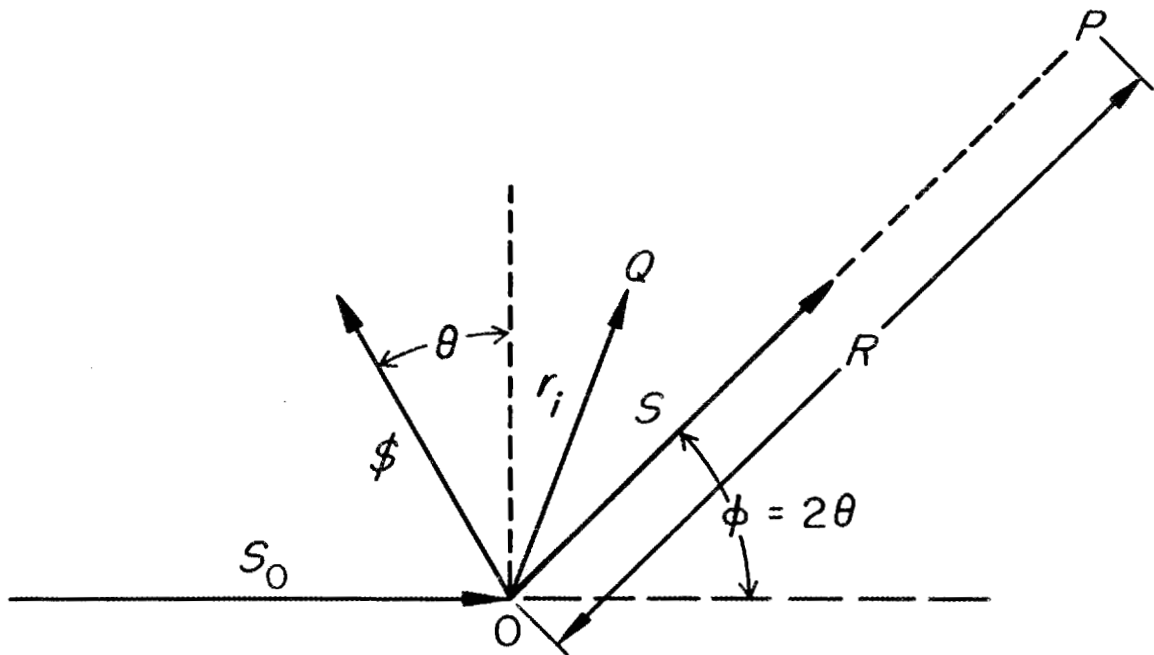


Fig. 6. The Scattering of X-Radiation by Electrons.

$$\underline{E}'_p = \underline{E}_0 e^2 / mc^2 R,$$

where \underline{E}_0 is a vector describing the amplitude of the incident beam, e is the electronic charge, m is the mass of the electron and c is the velocity of light. If there were z electrons at O , then the amplitude at P could be given by $z\underline{E}'_p$. However, since z electrons cannot be located at a single point and are spread out about an atom at distances comparable to the wavelength of the x-rays, interference effects result. Thus the resultant amplitude, for a spherical atom, is given by

$$\underline{E}_p = f(s) \underline{E}_0 e^2 / mc^2 R$$

where $f(s)$ is the atomic form factor which is a function of the distribution of the electrons about the atom and of the scattering angle (see (5.1.3)). The magnitude of $f(s)$ is equal or less than z , the atomic number.

Now consider the phase of radiation scattered by the electrons of atom i located at Q as compared to that scattered by an atom at O . In Fig. 6, the incident beam is defined by the unit vector \underline{S}_0 , and the scattered radiation in the direction OP by the unit vector \underline{S} . The vector \underline{S} is defined by the expression $\underline{S} - \underline{S}_0$, and \underline{r}_i is a vector denoting the distance OQ . The phase difference ψ of radiation coming from the two points O and Q is the path difference multiplied by $2\pi/\lambda$ or

$$\psi = - (2\pi/\lambda) \underline{r}_i \cdot \underline{S}.$$

If the incident wave is of the form

$$\underline{E} = \underline{E}_0 \exp(2\pi i \nu t)$$

where ν is the frequency and t time, then the amplitude at point P due to all atoms i becomes

$$\underline{E}_p = (\underline{E}_0 e^2 / mc^2 R) \sum_i f_i(s) \exp(2\pi i \nu t) \exp(2\pi i \underline{r}_i \cdot \underline{S} / \lambda).$$

In order to obtain the intensity of the waves arriving at P, the above equation must be multiplied by its complex conjugate, giving

$$E_p^2 = (E_0 e^2 / mc^2 R)^2 \sum_i \sum_j f_i(s) f_j(s) \exp(2\pi i (\underline{r}_i - \underline{r}_j) \cdot \underline{s} / \lambda).$$

Since E_p^2 is proportional to the intensity of scattered radiation, represented by I_p , and the factor $(E_0 e^2 / mc^2 R)^2$ is proportional to the intensity scattered by a single electron, represented by I_e , the preceding equation can be written as

$$I_{eu} = I_p / I_e = \sum_i \sum_j f_i(s) f_j(s) \exp(2\pi i (\underline{r}_i - \underline{r}_j) \cdot \underline{s} / \lambda). \quad (5.1.1)$$

Furthermore, \underline{s}_0 and \underline{s} are unit vectors; therefore the absolute value of \underline{s} is $2\sin\theta$, where θ is the half-scattering angle. Also if

$$\underline{r}_{ij} = \underline{r}_i - \underline{r}_j$$

then

$$\underline{r}_{ij} \cdot \underline{s} = r_{ij} s \cos \alpha$$

where α is the angle between the vectors \underline{r}_{ij} and \underline{s} . Thus, by substituting these quantities into (5.1.1),

$$I_{eu} = \sum_i \sum_j f_i(s) f_j(s) \exp(is r_{ij} \cos \alpha) \quad (5.1.2)$$

where s is defined as

$$s = (4\pi/\lambda) \sin \theta \quad (5.1.3)$$

In a liquid system all orientations of \underline{r}_{ij} are equally probable, and (5.1.2) must be integrated over all directions of \underline{r}_{ij} . The following equation results:

$$I_{eu} = \sum_i \sum_j f_i(s) f_j(s) \int_0^\pi \int_0^{2\pi} \exp(is r_{ij} \cos \alpha) \sin \alpha d\alpha d\varphi / \int_0^\pi \int_0^{2\pi} \sin \alpha d\alpha d\varphi$$

which yields upon evaluation

$$I_{eu} = \sum_i \sum_j f_i(s) f_j(s) \sin(sr_{ij}). \quad (5.1.4)$$

Here both summations range over all the atoms in the sample. Equation (5.1.4) is Debye's equation¹⁰ for the total intensity of a coherently scattered wave; the scattered intensity in electron units, I_{eu} , is a function of the scattering factors of the atoms, the interatomic distances, the wavelength of the x-radiation, and the scattering variable s .

In a polyatomic liquid, a certain group containing m atoms may be chosen as the stoichiometric unit. Let there be n such stoichiometric units in the sample. From (5.1.4) the scattered intensity can be written as

$$I_{eu} = n \sum_{i=1}^m f_i^2(s) + \sum_{i=1}^m \sum_{j=1}^{n \cdot m} f_i(s) f_j(s) \sin(sr_{ij})/sr_{ij} \quad (5.1.5)$$

Summation is now over the stoichiometric unit for i , and over all atoms in the sample for j .

5.2 Reduced Intensity and Radial Distribution Function (RDF)

The term I_{eu}/n in (5.1.5) represents the measured intensity, normalized to one stoichiometric unit of the sample. The reduced intensity $i(s)$, defined as

$$i(s) \equiv I_{eu}/n - \sum_i f_i^2(s) \quad (5.2.1)$$

is the structure sensitive part of the scattered intensity. The term

$\sum_i f_i^2(s)$ is the independent atomic scattering from the atoms in one stoichiometric unit.

* Index j now denotes all atoms in the system except for the chosen atom i ; thus the second term in (5.1.5) represents the intensity due only to the interaction between atom pairs.

If the pair distribution of j atoms around i atoms is expressed by $\rho_{ij}(r)$, then the number of atoms j contained in a spherical shell between r and $r + dr$ from an atom i is $4\pi r^2 \rho_{ij}$, and the summation of distances in (5.1.5) may be replaced by an integral

$$i(s) = \sum_i \sum_j f_i(s) f_j(s) \int_0^{\infty} 4\pi r^2 \rho_{ij}(r) \sin(sr) dr/sr \quad (5.2.2)$$

where the summations over both i and j are now over the stoichiometric unit. The kernels $r\rho_{ij}(r)$ tend to infinity at large r . For the application of the Fourier integral theorem, it is advantageous to add and to subtract from each term the quantity $r\rho_0$, ρ_0 being the uniform number density. Since $\rho_{ij}(r)$ is significantly different from ρ_0 only at small values of r , convergence is readily obtained, and Fourier inversion can be carried out:

$$i(s) = \sum_i \sum_j f_i(s) f_j(s) \left\{ \int_0^{\infty} 4\pi r^2 [\rho_{ij}(r) - \rho_0] \sin(sr) dr/sr + \int_0^{\infty} 4\pi r^2 \rho_0 \sin(sr) dr/sr \right\}.$$

The second term is very nearly zero except for very small s ; thus the equation may be written as

$$i(s) = \sum_i \sum_j f_i(s) f_j(s) \int_0^{\infty} 4\pi r^2 [\rho_{ij}(r) - \rho_0] \sin(sr) dr/sr \quad (5.2.3)$$

It is instructive for the following to consider the case where there is but one kind of atom. The sum in (5.2.3) is then a single term:

$$i(s) = f^2(s) \int_0^{\infty} 4\pi r^2 [\rho(r) - \rho_0] \sin(sr) dr/sr \quad (5.2.4)$$

Fourier inversion yields $\rho(r)$ in terms of the experimentally accessible reduced intensity, and the radial distribution function (RDF) becomes:

$$4\pi r^2 \rho(r) = 4\pi r^2 \rho_0 + (2r/\pi) \int_0^{\infty} [si(s)/f^2(s)] \sin(sr) ds \quad (5.2.5)$$

In the general case, an analogous treatment, while not yielding directly a radial pair distribution, does yield an interpretable function from which structural information can be inferred. One forms the Fourier transform of

$$i(s)M(s) = \sum_i \sum_j f_i(s)f_j(s)M(s) \int_0^{\infty} 4\pi r^2 [\rho_{ij}(r) - \rho_0] \sin(sr)/sr \, dr \quad (5.2.6)$$

in which the "modification function" $M(s)$ may be chosen at will, and in practice is chosen to make the factors $f_i(s)f_j(s)M(s)$ roughly independent of s . The use of modification functions is discussed thoroughly by Waser and Schomaker.¹¹ Fourier transformation of (5.2.6) yields a function

$$D(r) \equiv \sum_i \sum_j D_{ij}(r) = 4\pi r^2 \rho_0 + (2r/\pi) \int_0^{\infty} si(s)M(s) \sin(sr) \, ds \quad (5.2.7)$$

in which individual modified pair distribution functions $D_{ij}(r)$ are related to the $\rho_{ij}(r)$ in a known way¹¹:

$$D_{ij}(r) = 4\pi r \int_{-\infty}^{\infty} u \rho_{ij}(u) T_{ij}(u-r) \, du \quad (5.2.8)$$

$$T_{ij}(r) = (1/\pi) \int_0^{\infty} f_i(s)f_j(s)M(s) \cos(sr) \, ds \quad (5.2.9)$$

Thus $D(r)$, the function accessible from experiment (see section 6.7), is a kind of linear combination of true radial pair distributions which are convoluted with the known functions $T_{ij}(r)$ given by (5.2.9). The function $(r/r_0)T(r)$ may be thought of as representing the modified appearance in $D(r)$ of an idealized $\rho(r)$ having a single delta-function peak at $r = r_0$ (see also section 7.2).

6. PROCESSING OF DATA

6.1 The Raw Data

The data evaluation described in the following sections is done by a high speed computer. Provisions are made for the output of intermediate results, so that unforeseen difficulties in the data treatment can be dealt with as they occur.

Data taken on heavy water (D_2O) at $4^\circ C$ will be used to illustrate the remaining sections.

Fig. 7 shows the measured scattered intensity I^* in counts per minute as a function of s (defined in equation 5.1.3). As indicated in Fig. 7, each section is characterized by certain size divergence slits. Repeat runs have been averaged. The following equation is used to find the relative intensity at each s :

$$I_R(s) = [(I^* - I_B)/PA]_N - I_C \quad (6.1.1)$$

I_B is the correction for background radiation; P and A are the polarization and absorption correction factors. The subscript N is to indicate that the quantity in the brackets is at this stage normalized to one of the sections of a certain size divergence slits, usually that measured with the 1° beam divergence. The quantity I_C is the correction for incoherent or Compton scattering. These corrections will now be described in detail. Due to the high resolution of the monochromator, it is not necessary to correct for secondary fluorescent radiation (except for compounds containing the elements Br, Rb, Pb or U).

6.2 Background

Intensity I_B due to background radiation is measured for each section by placing a lead shutter in front of the scatter slit (6) in Fig. 2 with

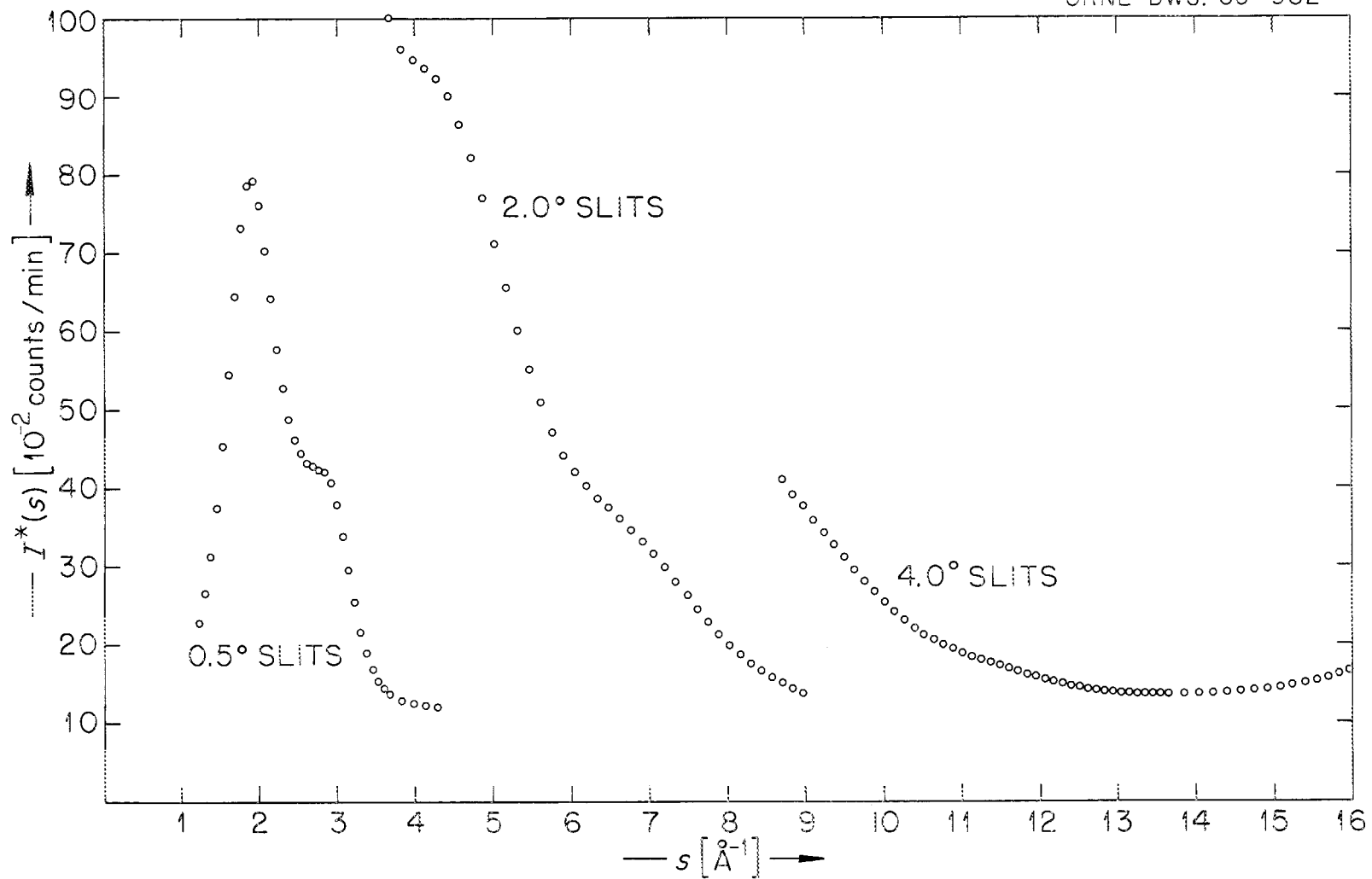


Fig. 7. Uncorrected Intensity Scattered from the Free Surface of Liquid D_2O , Measured with Three Different Divergence Slit Combinations.

the x-ray beam on. Typical values range from 2 counts per minute at low angles to 5 at high angles.

6.3 Polarization

For crystal-monochromatized radiation with a common plane of scattering at monochromator and sample a ray scattered by the sample is diminished in intensity by the factor

$$P = (1 + \cos^2 2\theta' \cos^2 2\theta) / (1 + \cos^2 2\theta) \quad (6.3.1)$$

in which θ' is the Bragg angle for the reflecting planes of the monochromatizing crystal. For the (200) planes of sodium chloride and MoK α radiation $\cos^2 2\theta'$ is 0.9375.

6.4 Absorption

The absorption correction to the diffracted intensity measured with the geometry of the described instrument is discussed in section 8.1.2. It is shown there that the factor A in equation (6.1.1) is given by

$$A = [1 - (1 - \exp(-x))/x] \quad (6.6.1)$$

where $x = 2\alpha\mu/\sin 2\theta$, with μ the linear absorption coefficient and α the beam divergence. As μ , and hence x , becomes large, the factor A approaches unity, the usual case.

6.5 Compton Scattering

The correction for Compton scattering is different from that for standard techniques, because of the location of the monochromator in the scattered beam (Fig. 1 and 2). The Compton scattering for this geometry is a rapidly rising function at small angles, where characteristic radiation is the exciting source. With increasing scattering angle the difference between the wavelength of the exciting source for Compton scattering and the

wavelength selected by the monochromator increases. Thus the exciting source for incoherent scattering shifts to shorter wavelengths until, eventually, the continuum serves as the exciting source for the observed Compton scattering. The non-discrete width of the exciting source contributes also to the shape of the Compton scattering curve.

The result is a function which rises approximately as the theoretical¹² Compton scattering function at small angles and then falls rapidly. Its contribution at large angles is a small part of the total intensity.

A semi-empirical procedure has been followed in order to obtain the detailed shape of the Compton scattering curve. The Compton scattering correction is a low-frequency term in the reduced intensity function $i(s)$. Its Fourier transform is therefore a peak at small distances in the RDF $D(r)$ (see section 5.2). The reduced intensity function i_1 is first transformed to obtain an RDF D_1 . D_1 is then re-inverted with cut-off at a fixed value in the radial distance r to give a reduced intensity i_2 . Values of D_1 up to the region of the first important peak in the RDF are then set equal to zero, and this RDF D_1^{\dagger} is re-inverted once more with the cut-off at the same value of r as for the previous inversion, giving a reduced intensity i_2^{\dagger} . The basic assumption is here that there are no atom pair interactions in the RDF at distances r shorter than interatomic distances. The difference between the two reduced intensity functions i_2 and i_2^{\dagger} gives a correction curve with the effect of the high angle cut-off removed.

This procedure was carried out in a study of liquid water at room temperature. Once the shape $I_C^0(s)$ of the Compton scattering correction has been established, similar curves can be obtained for other studies through proper normalization and correction for differences in inelastic scattering factors. The shape of the Compton correction curve is shown in Fig. 8,

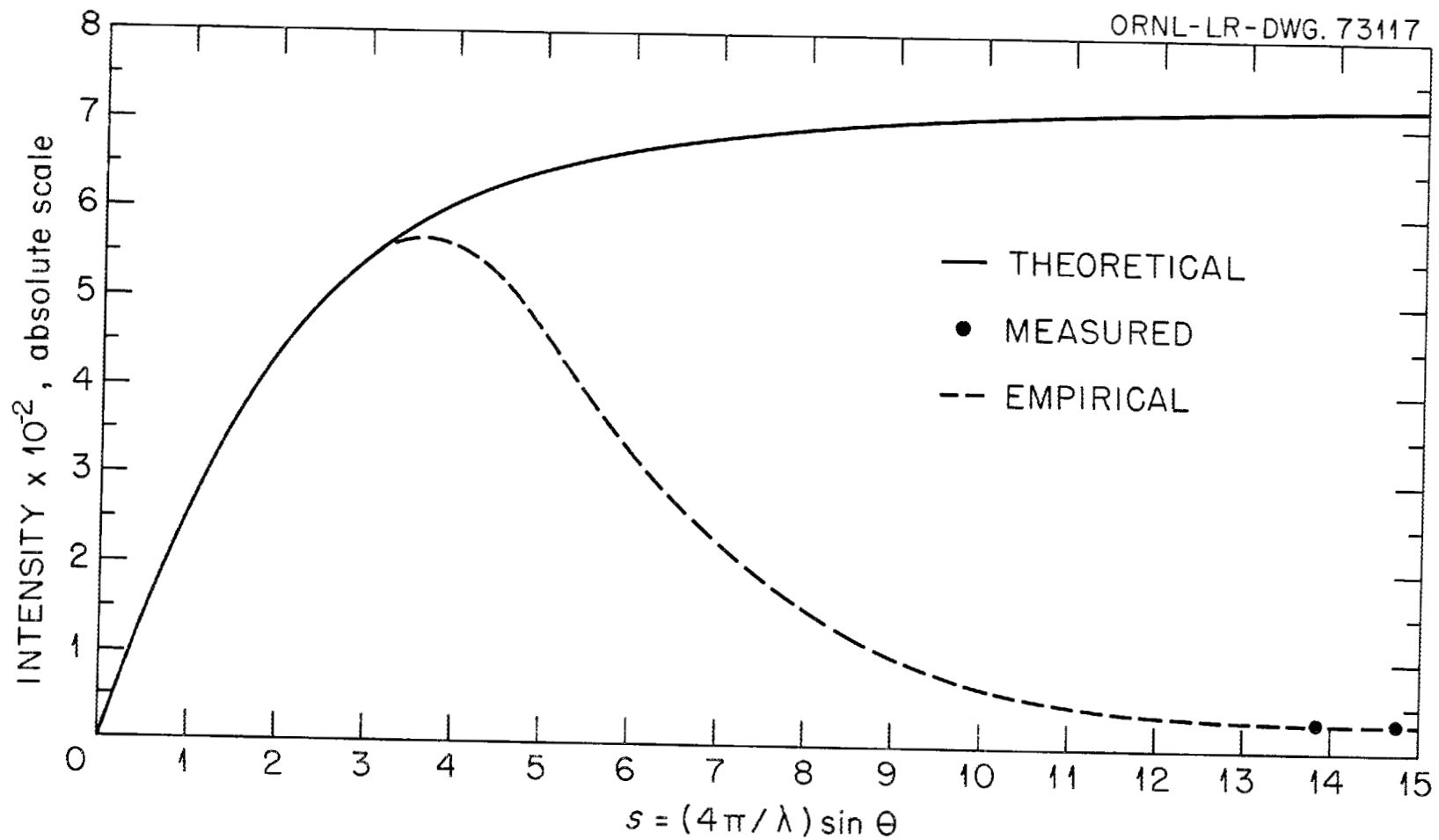


Fig. 8. Compton Scattering, H₂O.

along with the theoretical curve which would apply in the normal arrangement (source monochromatized).

The Compton scattering, in the present case, can be measured at large scattering angles. It is in this region that the absolute intensity scale is established (see section 6.6). A Zr filter (0.004") is first placed between x-ray source and sample, with the scattering angle well above that required for cut-off of the exciting radiation by the Zr edge (about $\theta = 40^\circ$), and the scattered intensity is measured. There should be, in this case, no contribution from Compton scattering. Another measurement is then taken at the same scattering angle with the Zr filter between sample and detector. The total scattering, attenuated by the filter, is transmitted in this case. From these measurements, the fraction of Compton scattering can be obtained as well as its contribution at the unfiltered level.

The Compton scattering I_C in (6.1.1) for any liquid (superscript 1) is obtained from the standard curve shape (superscript 0) and the measured value at $s = \sigma$, using the expression

$$I_C^1(s) = I_C^0(s) \frac{I_C^1(\sigma)}{I_C^0(\sigma)} \frac{[\sum_i F_i^2]^1}{[\sum_i F_i^2]^0} \quad (6.5.1)$$

The quantities within the brackets are the incoherent scattering factors for the components of substances 1 and 0, summed over the stoichiometric unit.

6.6 Normalization

The corrected relative intensities $I_R(s)$ from the preceding steps (equation 6.1.1) are now placed on an absolute basis by normalizing at high angles to the theoretical scattering arising from independent atoms, $\sum_i f_i^2(s)$, contained in the stoichiometric unit. The angle chosen for normalization is the same as that corresponding to $s = \sigma$, where the Compton scattering was measured (see section 6.5).

Alternative methods for scaling the observed diffraction data have been proposed and discussed¹³. In an extension of this work, Rahman¹⁴ has derived an equation which makes use of the whole measured intensity (although also placing heavy weight on the high angle region) for the computation of the normalization constant C . We prefer to use the high angle scaling factor in our work, but the normalization constant derived from Rahman's equation¹⁴ is always compared with the high angle value. The difference between the C -values derived by the two methods (which, for our work, has never exceeded 5%) is our basis for assigning an error to the scaling factor C . The total scattered intensity in electron units (equation 5.1.4) is obtained from

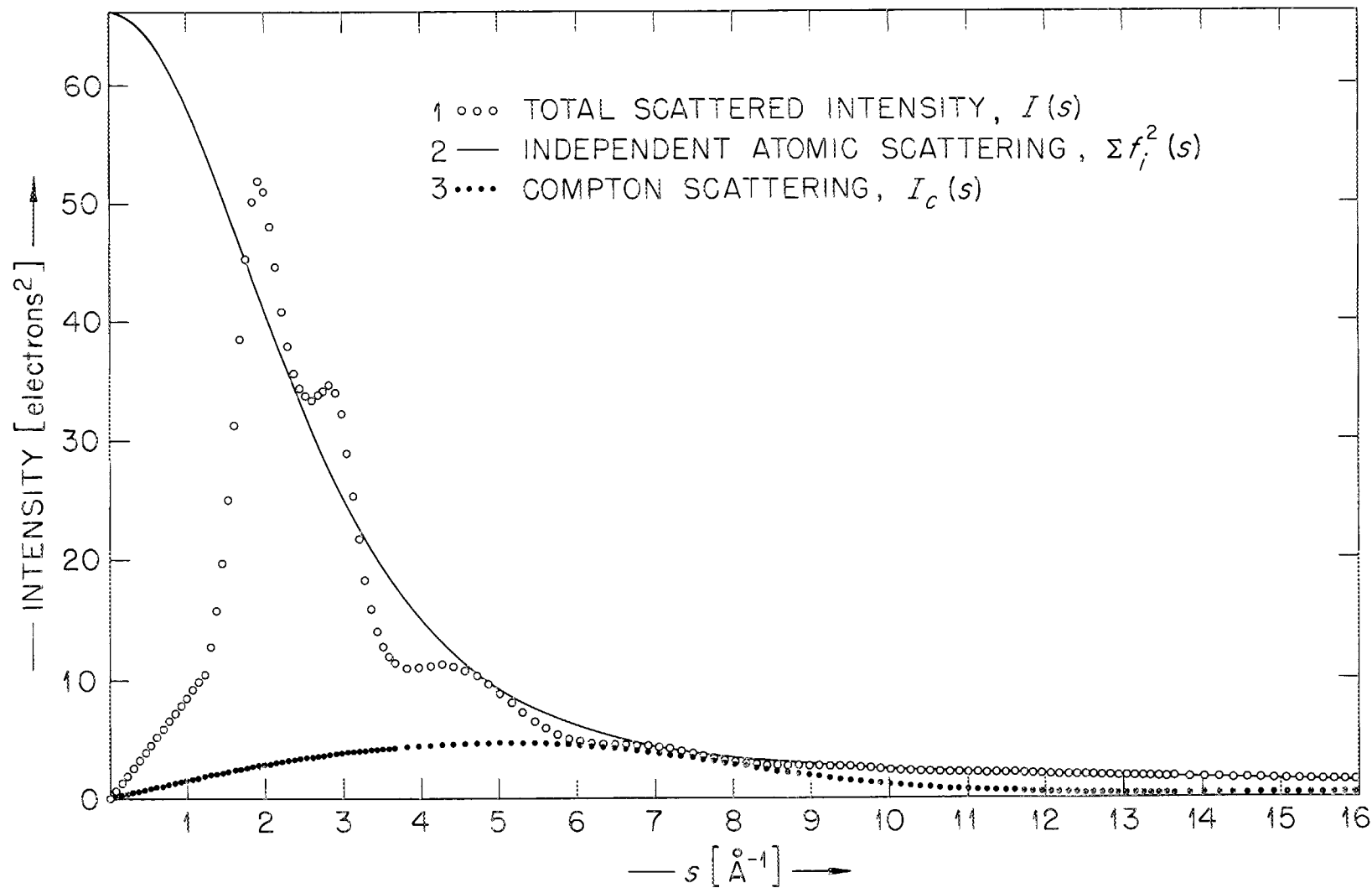
$$I(s) = C I_R(s) \quad . \quad (6.6.1)$$

It is shown in curve 1 of Fig. 9, together with the independent atomic scattering (curve 2, Fig. 9), and the Compton scattering (curve 3, Fig. 9).

6.7 Reduced Intensity and Radial Distribution Function (RDF)

The reduced intensity $i(s)$ represents the structurally sensitive part of the total coherent intensity. It is computed from

$$i(s) = \left[I(s) - \sum_i f_i^2(s) \right] \quad (6.7.1)$$

Fig. 9. Corrected and Normalized Scattered Intensity (D₂O).

The modification function $M(s)$ has been discussed in section 5.2; it has also been shown there that the reduced intensity function is related to the RDF by the expressions

$$D(r) \equiv 4\pi r^2 \rho_0 + (2r/\pi) \int_0^{\infty} \text{si}(s) M(s) \sin(sr) ds \quad (5.2.6)$$

which are repeated here for convenience.

An inevitable limitation of experimental intensity functions is the absence of data above a maximum accessible value of s . The effect on $D(r)$ of this cut-off can be understood through the incorporation of the cut-off into $M(s)$ and thus inclusion in the functions $T_{ij}(r)$, as discussed in section 5.2.

Another, less critical limitation is the absence of data below a minimum accessible value of s (see section 4). The experimental intensity function $I(s)$ can be extrapolated to zero angle by fitting a polynomial to the observed part of the curve. If a model intensity function (see section 7.2) can be computed in agreement with the observed part of the curve, then this model function can be used for extrapolation to $s = 0$. In the example of D_2O , both procedures lead to the same result.*

The reduced intensity curve for our example, computed from (6.7.1), is shown in Fig. 10. A low-frequency perturbation of the curve is clearly recognizable. This perturbation may be caused by incorrect data treatment (sections 6.1 to 6.7), by the use of incorrect atomic scattering factors, or by an apparatus function. It will cause a peak at small distances r in the RDF. The perturbation can be removed by repeated Fourier transformations as discussed in section 6.5.

* At very small values of s , the behavior of the reduced intensity is determined by the isothermal compressibility, β_T :¹⁵

$$\text{si}(s) \approx (\beta_T - 1)s \approx -s$$

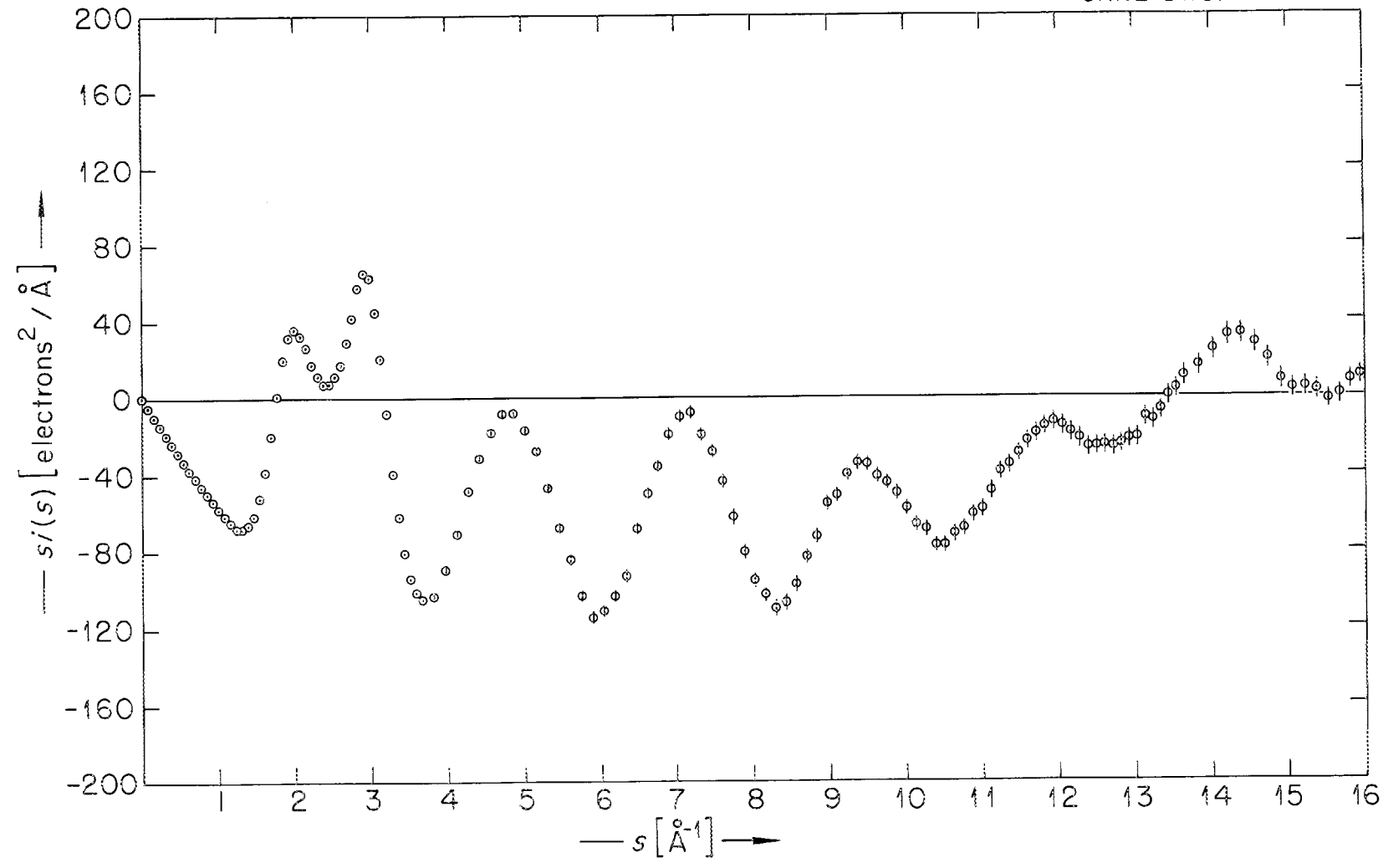


Fig. 10. Reduced Intensity (D_2O).

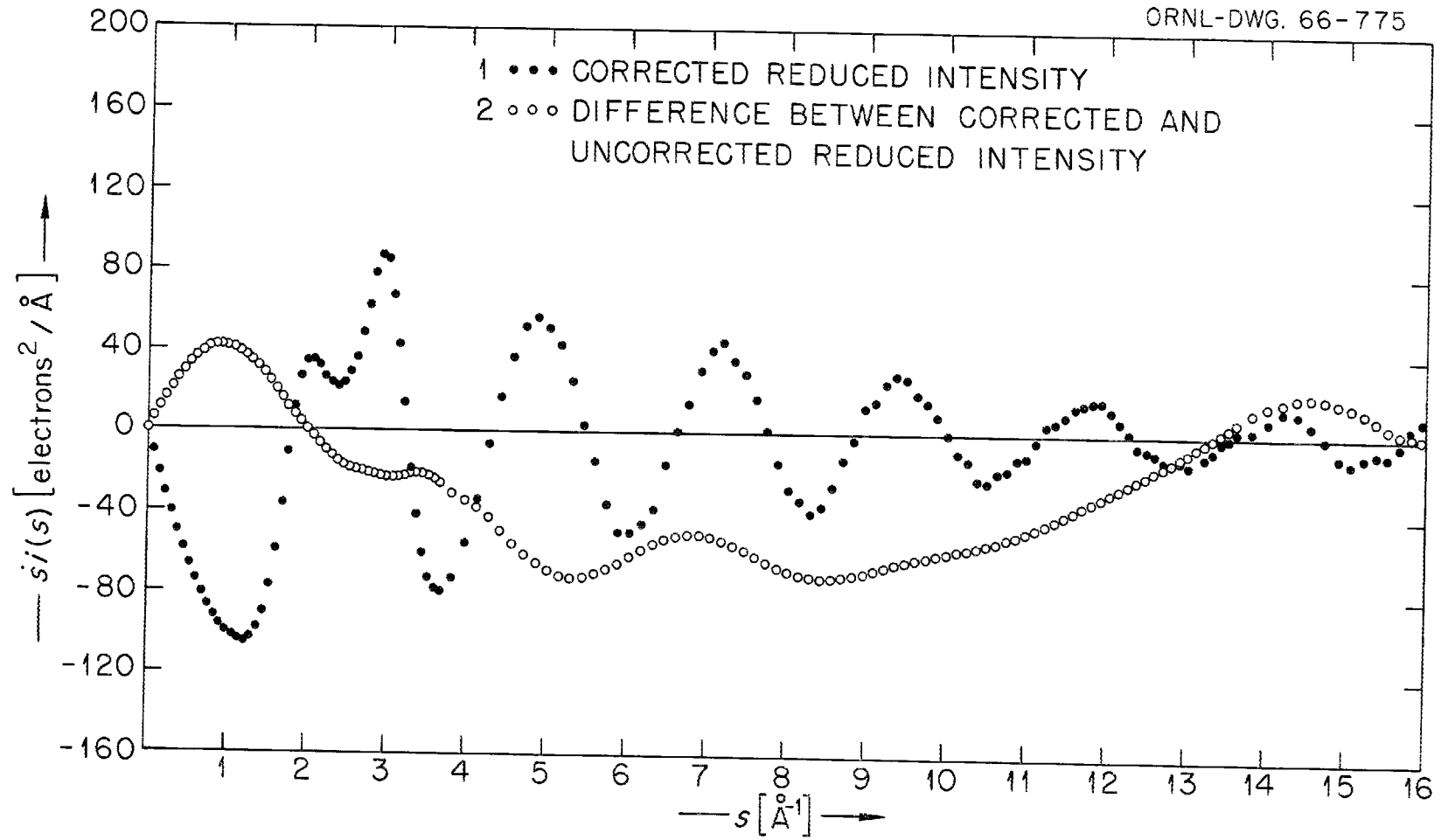


Fig. 11. Corrected Reduced Intensity (D₂O).

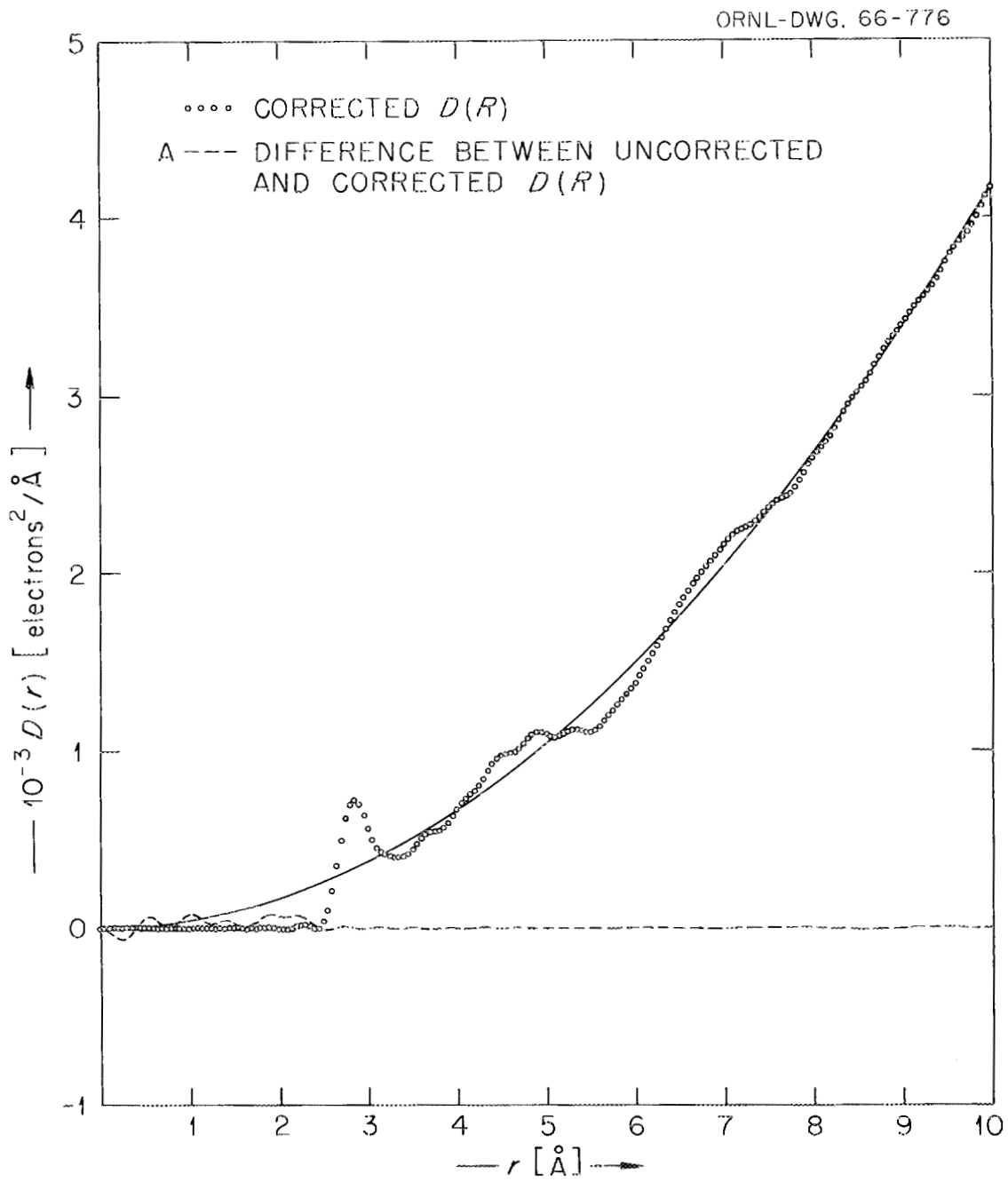


Fig. 12. Corrected Radial Distribution Function (D_2O).

Curve 1 in Fig. 11 is the final reduced intensity $s_i(s)$ referred to in the following sections. Curve 2 (Fig. 11) is the low-frequency correction term which has been subtracted from the original curve of Fig. 10. Fig. 12 shows the RDF with the removed correction term shown in curve A. In this particular example, part of the correction term is due to the O-D interactions around $r = 1 \text{ \AA}$, which were neglected in this study because of the low x-ray scattering amplitude of the one electron in the hydrogen atom.

7. INTERPRETATION OF DATA

The behavior of any fluid is a consequence of its molecular structure, which, in the equilibrium state, is most conveniently described by the RDF. For systems interacting with short-range, two-body central forces, accurate knowledge of the RDF, the intermolecular potential, and the intramolecular energy states provides a solution to all thermodynamical problems¹⁵. In the absence of this information, the experimental determination of reduced intensity and radial distribution functions is of prime importance for our understanding of the liquid state as well as of the structure of molecules in liquid solution.

7.1 Simple Liquids

The calculation of radial distribution functions from known or assumed intermolecular potentials is one of the most difficult problems in statistical mechanics. It has been solved only for model systems. Even qualitative agreement with experiment has been achieved only for the simplest classical fluid, argon¹⁶.

If the RDF is known from experiment, it can be used to derive the intermolecular potential. Even this procedure is feasible only for simple

liquids, i.e. systems interacting with short-range, two-body central forces. Born and Green¹⁷ have shown that there is an exact relation between the pair correlation function n_2 , the third-order distribution function n_3 , and the pair potential* ϕ . The pair correlation function can be written

$$n_2(r) = \rho_0^2 \exp(-U(r)/kT) \quad (7.1.4)$$

* If $d\tilde{x}^{(1)}, d\tilde{x}^{(2)}, \dots, d\tilde{x}^{(q)}$ is a set of q distinct volume elements situated at the positions $\tilde{x}^{(1)}, \tilde{x}^{(2)}, \dots, \tilde{x}^{(q)}$ in a fluid, then the probability that each of these is simultaneously occupied by a molecule, will be proportional to $d\tilde{x}^{(1)}d\tilde{x}^{(2)}\dots d\tilde{x}^{(q)}$, and can therefore be represented by $n_q d\tilde{x}^{(1)}d\tilde{x}^{(2)}\dots d\tilde{x}^{(q)}$. When $q = 1$, n_q is simply the number density of the molecules, already defined as ρ_0 ; when $q = 2$, n_q is the probability of finding molecules simultaneously at two given points separated by a distance r . The distribution function $\rho(r)$ used in section 5 is the probability of finding molecules separated by a distance r if one of the molecules has the position $r = 0$, or

$$\rho(r) = n_2(r)/n_1(r) = n_2(r)/\rho_0 \quad (7.1.1)$$

The pair distribution function is therefore the most important of the distribution functions and it is often convenient to introduce a normalized pair correlation function $g(r)$, which approaches unity for large values of r . This is related to n_2 by

$$n_2(r) = \rho_0^2 g(r) \quad (7.1.2)$$

in an isotropic fluid; the pair correlation function is related to $D(r)$ by

$$D(r) = 4\pi r^2 \rho_0 g(r) \quad (7.1.3)$$

(if $f_i(s) f_j(s) M(s) = 1$).

where $U(r)$ is a potential of mean force defined by (7.1.4). Then we have¹⁸

$$\frac{\partial U(r_2 - r_1)}{\partial r_1} = \frac{\partial \phi(r_2 - r_1)}{\partial r_1} + \int [n_3(r_1, r_2, r_3) / n_2(r_1, r_2)] \frac{\partial \phi(r_3 - r_1)}{\partial r_1} dr_3 \quad (7.1.5)$$

$\phi(r)$ can, however, only be derived from $U(r)$ and equation (7.1.5) if n_3 is known. A serious approximation has to be made at this point, namely

$$\rho_0^3 n_3(r_1, r_2, r_3) = n_2(r_1, r_2) n_2(r_1, r_3) n_2(r_2, r_3) \quad (7.1.6)$$

which is the superposition approximation of Kirkwood¹⁹. From (7.1.5) and (7.1.6) an integral equation for $\phi(r)$ can be obtained¹⁸:

$$\phi(r) = U(r) + (\pi/\rho_0^3 r) \int_0^\infty [n_2(u) \frac{\partial \phi(u)}{\partial u}] du \int_{-u}^u (u^2 - v^2)(v+r) [n_2(|v+r|) - \rho_0^2] dv \quad (7.1.7)$$

where u and v are dummy variables. Equation (7.1.7) can be solved numerically for the pair potential $\phi(r)$ if $n_2(r)$ is known from diffraction experiments. The discovery of oscillatory interaction between ions in liquid metals is an example²⁰ of the method described.

Unfortunately, this method has serious limitations. The validity of the superposition approximation (equation (7.1.6)) has been questioned even for liquid argon²¹. Also, the pair potential $\phi(r)$ is very sensitive to the form of the RDF at small distances r . Very accurate diffraction data are necessary in order to obtain more than qualitative knowledge of the intermolecular potential.

7.2 Complex Liquids

For complex fluids consisting of polyatomic molecules whose interaction cannot be described by a sum of pair potentials, a less ambitious course has to be followed. In a broader and, to many, a more interesting sense, the RDF represents only the beginning of a description of the structure of such a liquid. The broader problem is to infer from the RDF something of the

typical atomic arrangement in a liquid, insofar as this is non-random. In dealing with this aspect of the problem, it is important that the RDF is an average of any actual instantaneous distribution over a volume large to atomic dimensions. Since the instantaneous environments of different but chemically equivalent atoms may well be quite different one from another, it must not be concluded that the RDF uniquely describes the environment of all atoms of a given type. A further source of difficulty in interpreting $D(r)$ lies in the nature of the features it contains: Individual peaks in $D(r)$ characteristically have widths which are of comparable magnitude to their separation from one another. Thus one encounters uncertainty in evaluating the number of atomic pair interactions represented by a given feature of $D(r)$, and some arbitrary criterion must usually be applied. For a particular liquid, information on the atomic arrangement in the solid state, or on the structure of its molecules in the gas phase may be used for a preliminary analysis of the peak shape of the RDF. A definite molecular structure may then be proposed. For a liquid, this model structure may be assumed to be surrounded by a medium of constant average density. An intensity function may then be computed for the model structure and compared with that derived from experiment.*

$D(r)$, the function accessible from experiment, is a kind of linear combination of true radial pair distributions which are convoluted with the known functions $T_{ij}(r)$ given by equation (5.2.9). The function $(r/r_0)T(r)$ may be thought of as representing the modified appearance in $D(r)$ of an idealized $\rho(r)$ having a single delta-function peak at $r = r_0$. In order to extract information from $D(r)$ in a sound and expeditious way, it is useful

* In the following, discussion will be restricted to models which can be described by discrete interactions, extending to a radial distance r_0 , with no structure beyond this distance.

to compute, for each type of pair interaction present in the structure, the function $(r/r_0)T_{ij}(r)$, or more usually $(r/r_0)T_{ij}(r)$ convoluted with a Gaussian function. The result is often called a standard peak, or a synthetic peak:

$$D_{ij}(r) = 4\pi r^2 \rho_0 + (rc_{ij}/r_{ij}\pi) \int_0^{\infty} f_i(s)f_j(s)\exp(-b_{ij}s^2)M(s)[\cos(r-r_{ij})s - \cos(r+r_{ij})s]ds \quad (7.2.1)$$

where c_{ij} is the coefficient for the number of identical interactions, r_{ij} is the distance between atoms i and j , $M(s)$ is the modification function and b_{ij} is the temperature factor*.

*The distance r_{ij} separating each atom pair in a liquid is not rigidly maintained; thus for a non-rigid molecule where rotation is not considered, the distribution of distances would be expressed by the Gaussian distribution

$$(4b_{ij}\pi)^{-\frac{1}{2}} \exp[-(r-r_{ij})^2/4b_{ij}] \quad (7.2.2)$$

where $(r-r_{ij})$ is the difference between any value r_{ij} and its average. The transform of this Gaussian is another Gaussian, $\exp(-b_{ij}s^2)$, called the temperature factor. The coefficient b_{ij} is one-half the mean square variation in r_{ij} . This makes the contributions $D_{ij}(r)$ by atom pairs ij the resultant of the Gaussian distribution of distances (7.2.2) and the transform $T_{ij}(r)$. Therefore each term of (5.1.5), multiplied by its temperature factor and a modification function, becomes

$$si(s) M(s) = \sum_i \sum_j f_i(s)f_j(s) \exp(-b_{ij}s^2) M(s) \sin(sr_{ij})/r_{ij} \quad (7.2.3)$$

If only interactions of type ij are considered, then substitution of (7.2.3) into (5.2.7) yields

$$D_{ij}(r) = 4\pi r^2 \rho_0 + (2r/\pi) \int_0^{\infty} f_i(s)f_j(s)M(s)\exp(-b_{ij}s^2)\sin(sr_{ij})/sr_{ij} ds \quad (7.2.4)$$

By using the appropriate trigonometric identity (7.2.4) may be written as (7.2.1). Comparison of (7.2.1) with (5.2.8) results in the identity:

$$D_{ij}(r) - 4\pi r^2 \rho_o = (r/r_{ij})[T(r-r_{ij}) - T(r+r_{ij})]$$

Thus for the case where atom i interacts with atom j , $D_{ij}(r) - 4\pi r^2 \rho_o$ may be considered as the generalized peak shape. The second term on the right side of the above equation, though centered on the other side of the origin at $r = -r_{ij}$, may be of importance for small values of r_{ij} , as some of the features of $T(r+r_{ij})$ may extend across the origin.

The reduced intensity for a proposed model system can be written as the sum of two types of terms. The first type would represent the intensity from interactions at distances r_{ij} of the discrete structure and the second the intensity from interactions caused by a continuous distribution of distances (continuum) of the type ij beginning at r_{ij0} and extending to the limits of the liquid. Integrating equation (5.2.6) from $r = 0$ to $r = r_{ij0}$, with $\rho_{ij}(r) = 0$, and then from $r = r_{ij0}$ to infinity, with $\rho_{ij} = \rho_o$, the following equation may be written:

$$\begin{aligned} \text{si}(s)M(s) = & \sum_i \sum_j M(s) \exp(-b_{ij}s^2) f_i(s)f_j(s) \sin(sr_{ij})/r_{ij} \\ & + \sum_i \sum_j M(s) \exp(-b_{ij0}s^2) f_i(s)f_j(s) 4\pi\rho_o [sr_{ij0} \cos(sr_{ij0}) - \sin(sr_{ij0})]/s^2 \end{aligned} \quad (7.2.5)$$

where for the first set of terms, i is summed over the stoichiometric unit and j over all atoms contained in the discrete structure, and for the second set i and j are summed over the stoichiometric unit.

The second term in (7.2.5) arises from the integration of equation (5.2.6); it amounts to making a "hole" in a uniform structureless medium in which to

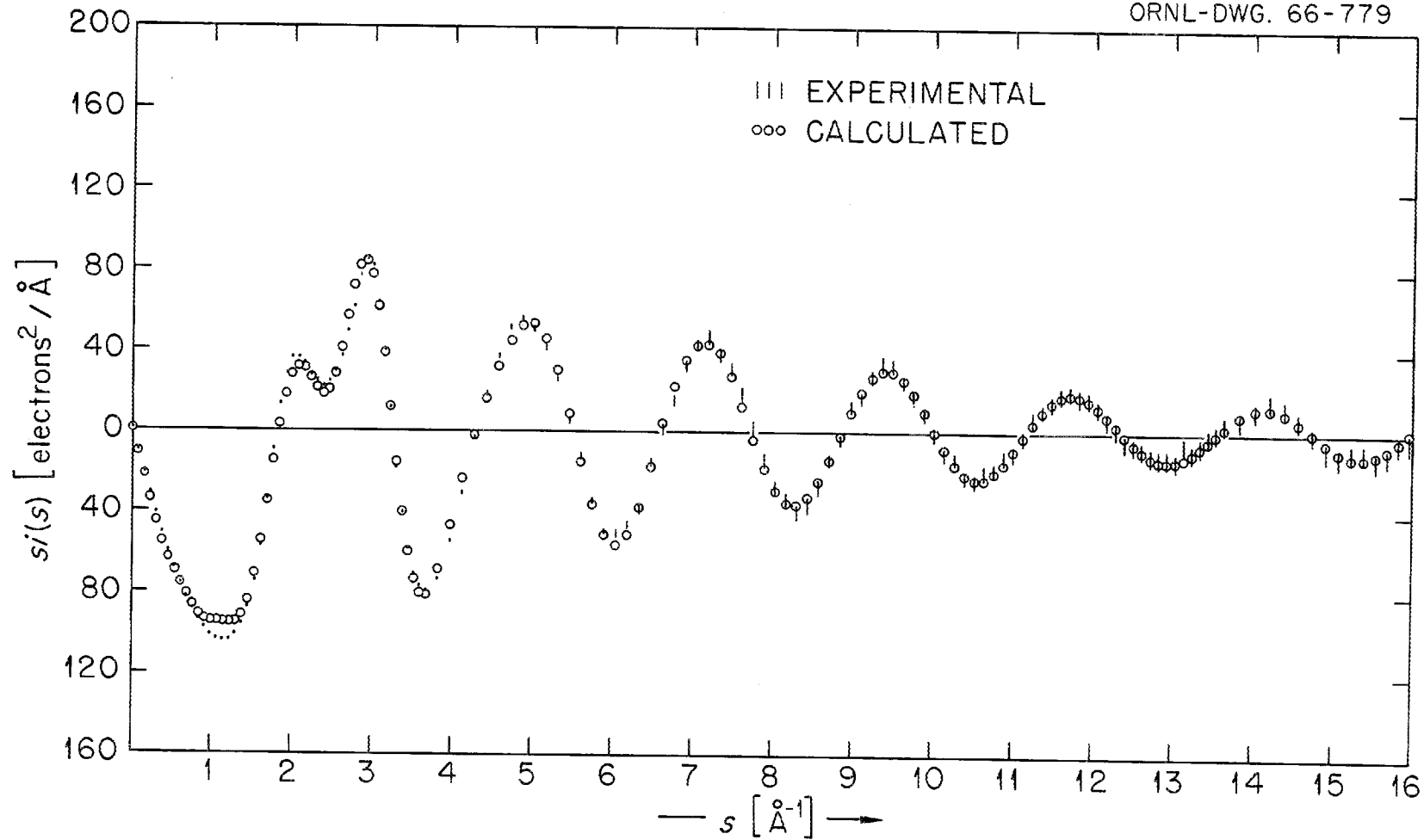


Fig. 13. Observed and Model Reduced Intensity (D_2O).

place the discrete interactions represented by the first term in (7.2.5). A temperature factor b_{ij0} is included in the second term since the emergence of the continuum will not be sharp. A close approximation for a given r_{ij0} can be made by assuming a homogeneous distribution of atoms. If n refers to the number of pairs of type ij contained in the discrete structure, then the radius of the volume containing n/ρ_0 atoms about i is the radius r_{ij0} at which the continuum is assumed to start: $r_{ij0} = (3n/4\pi\rho_0)^{1/3}$.

The model intensity function (7.2.5) may then be systematically refined to yield a satisfactory fit of the experimental data over the whole angular range. We have used an existing non-linear least squares program²², suitably modified for the purpose, for the refinement of the r and b values in (7.2.5).

Fig. 13 shows the experimental and model reduced intensity functions for the example D_2O . Fig. 14 presents the corresponding radial distribution functions obtained by Fourier inversion. The model structure used in the example is that for water proposed by Danford and Levy²³, with slight modifications in the model distances and temperature factors.

The temperature factors b_{ij} for a model distance r_{ij} are equal to one-half the mean square displacement in r_{ij} . In a case where the r_{ij} represent interactions between atoms inside a discrete molecule, the corresponding b_{ij} 's can be used²⁴ (in conjunction with spectroscopic data) for the assignment of vibrational frequencies in liquids.

7.3 Solutions

Liquid solutions containing several chemically different atoms, ions, or atom groups (molten salts may be included in this category²⁵) present special problems. For a binary solution with only two kinds of atoms, there are three terms in the sum in equation (5.2.3) or (5.2.7). The interpretation of $D(r)$ therefore requires the assignment of a given feature to one or

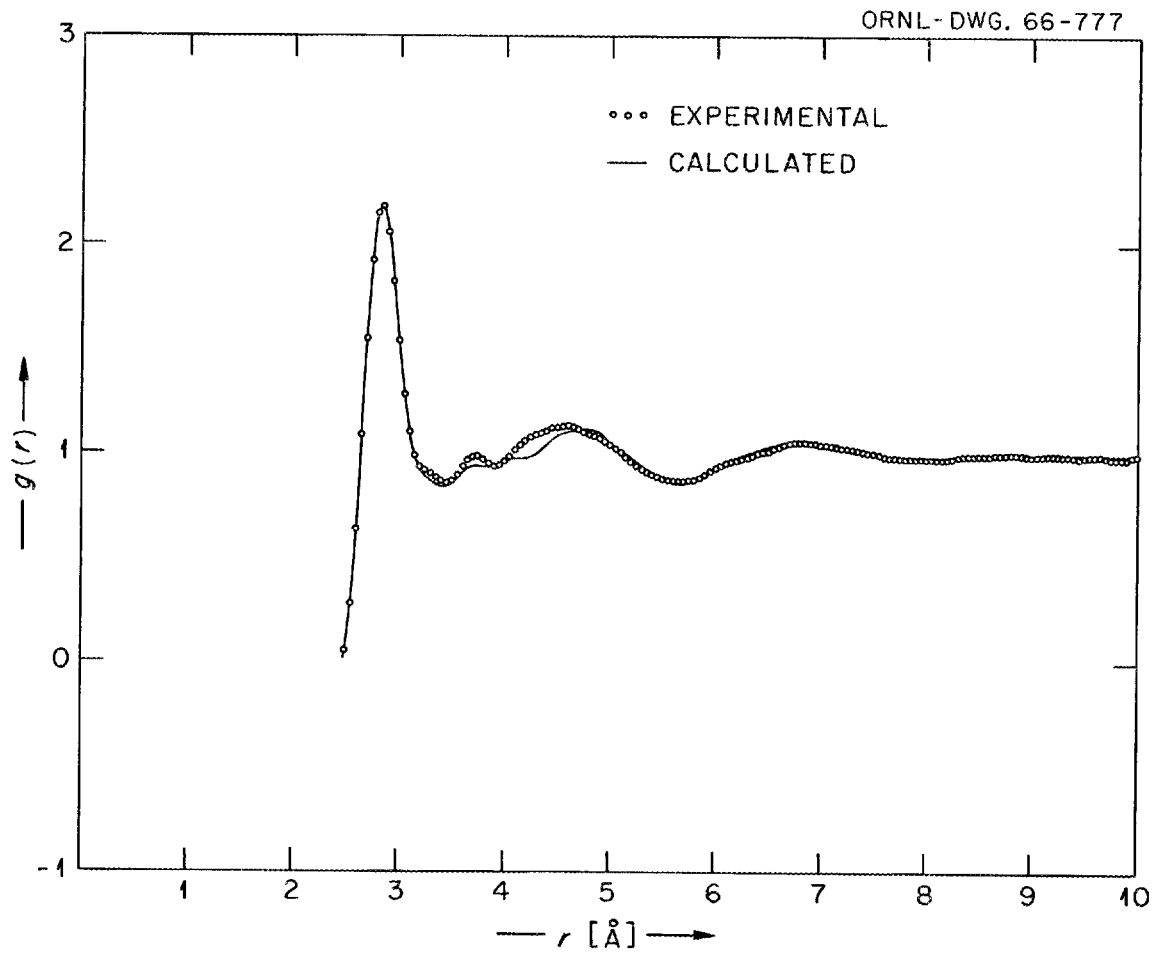


Fig. 14. Observed and Model Radial Distribution Function (D_2O).

another of the three terms, an assignment which must be made by an appeal to a structural model.²⁶

If enough independent measurements of the scattered intensity from such a system could be made, in which sufficiently different scattering factors apply, the resolution of $D(r)$ into separate, essentially unmodified pair correlation functions $\rho(r)$ would be feasible. Neutron diffraction studies with different isotopes seem promising in this respect.

8. APPENDIX

8.1 Absorption Corrections for a Flat Sample

The absorption correction to be applied to diffraction from a flat sample is given by $(1/2\mu)$, where μ is the linear absorption coefficient, and is easily developed for a single ray or a parallel sheath falling on a flat, highly absorbing sample²⁷.

The present problem is to find the proper absorption correction for the divergent beam technique under reasonable simplifying assumptions.

8.1.1 Highly Absorbing Samples. Fig. 15 shows the geometry of the problem.

A beam of divergence δ originating from a line source at X, falls on a flat sample at A, is diffracted and is measured at S_3 . The central ray XAS_3 makes equal angles θ of incidence and diffraction at the sample surface and thus has a scattering angle 2θ . The total path of a general ray through the sample deviating from the central ray by angle α , and diffracted at depth t is given by $t[\csc(\theta-\alpha)+\csc(\theta+\alpha)]$. If the intensity of the beam falling on the volume element dV at P is I_0 , the contribution to the scattered intensity from dV is given by $I_0 K \exp\{-t\mu[\csc(\theta-\alpha)+\csc(\theta+\alpha)]\} dV$. The factor K includes the constants and usual angle functions for diffracted intensities. The volume element dV will be taken as $WR^2 dR^2 d\alpha$, where W is the width of the beam. Since

ORNL-LR-DWG. 15719A

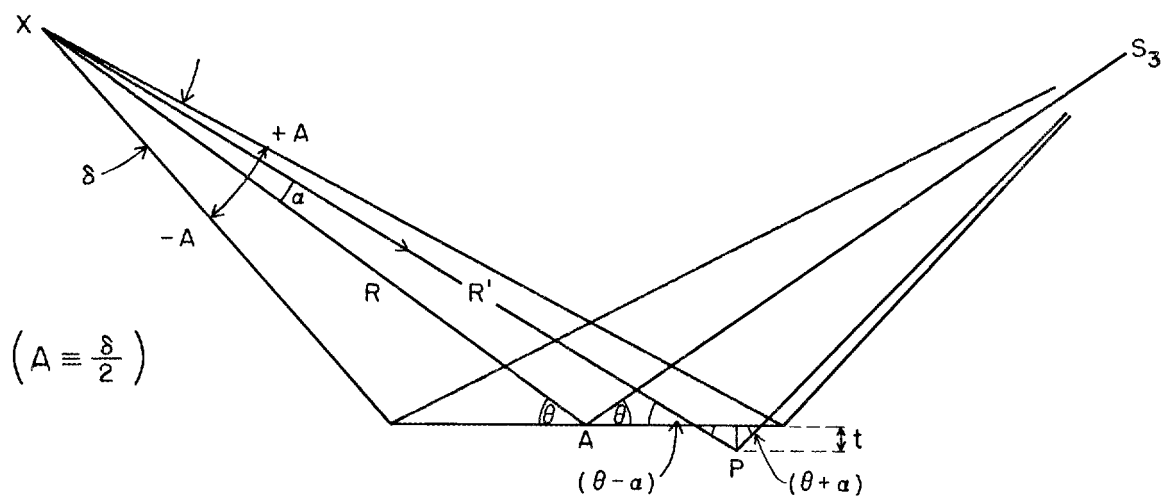


Fig. 15. Absorption Conditions for a Divergent Beam on a Highly Absorbing Flat Sample.

the point P is assumed to be a small distance below the surface of the sample, R' can be replaced by $R \sin \theta / \sin(\theta - \alpha)$. The element dR' can be replaced by $\csc(\theta - \alpha)dt$. Making these substitutions and introducing the proper limits of integration gives the expression for the scattered intensity I , properly corrected for absorption:

$$I = \int_{-A}^A \int_0^{\infty} I_0 W K \exp\{-t\mu[\csc(\theta+\alpha)+\csc(\theta-\alpha)]R \sin \theta \csc(\theta-\alpha)\} dt d\alpha / \sin(\theta-\alpha) \quad (8.1.1.1)$$

which on integration with respect to t yields:

$$I(\mu, \theta) = (WKR \sin \theta / \mu) \int_{-A}^A I_0 d\alpha / \sin^2(\theta-\alpha) [\csc(\theta-\alpha) + \csc(\theta+\alpha)] \quad (8.1.1.2)$$

Treating I_0 as constant, (8.1.1.2) can be written

$$I(\mu, \theta) = (I_0 WKR / 2\mu) \left\{ \int_{-A}^A 2 \sin \theta d\alpha / \sin(\theta-\alpha) - \int_{-A}^A d\alpha / \cos \alpha \right\}$$

which is then integrated to give

$$I(\mu, \theta) = (I_0 WKR / 2\mu) \left[2 \sin \theta \ln \left(\frac{\sin \theta + \sin A}{\sin \theta - \sin A} \right) + \ln \left(\frac{1 - \sin A}{1 + \sin A} \right) \right]$$

Finally, making use of the condition that $A \ll \theta$, this becomes

$$I(\mu) = I_0 WKA / \mu$$

The absorption correction is independent of the scattering angle if the intensity of the incident beam constant with respect to α .

Treating I_0 as a function of α , (8.1.1.2) can be written

$$I(\mu, \theta) = (WKR / 2\mu) \int_{-A}^A [2I_0(\alpha) \sin \theta / \sin(\theta-\alpha) - I_0(\alpha) / \cos \alpha] d\alpha$$

which can be put in the form

$$I(\mu, \theta) = (WKR / 2\mu) \int_{-A}^A [2I_0(\alpha) / \cos \alpha (1 - \cot \theta \tan \alpha) - I_0(\alpha) / \cos \alpha] d\alpha$$

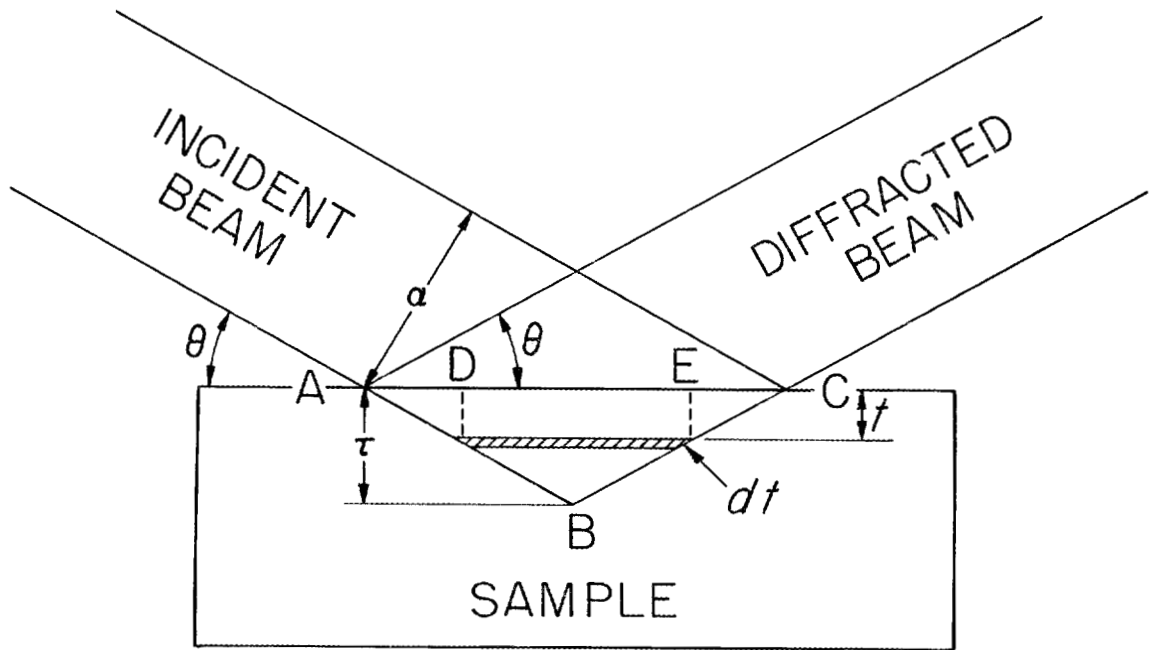


Fig. 16. Absorption Condition for Parallel Beam on a Deeply Penetrated Sample.

The factor $(1 - \text{ctn}\theta \tan \alpha)^{-1}$ can be expanded by the binomial theorem. Only the first two terms are retained, since the two conditions $\alpha \ll \theta$ and $0 < \theta \leq 90^\circ$ cause the term $(\text{ctn}\theta \tan \alpha)$ to be small compared to unity. If we use the approximations $\cos \alpha = 1$ and $\tan \alpha = \alpha$, we obtain

$$I(\mu, \theta) = (\text{WKR}/2\mu) \left\{ \int_{-A}^A I_0(\alpha) d\alpha + 2\text{ctn}\theta \int_{-A}^A \alpha I_0(\alpha) d\alpha \right\} .$$

If $I_0(\alpha)$ is an even function (beam is symmetrical about its center) the second integral in the above equation becomes zero. This also gives the important result that the absorption correction is independent of scattering angle. If there is a contribution to $I(\alpha)$ which is an odd function of α , then the term containing $\text{ctn}\theta$ remains, and the absorption correction is dependent on the scattering angle.

8.1.2 Deeply Penetrated Samples. For obtaining quantitative intensities from samples which are deeply penetrated, especially liquid and vitreous materials, for which impaired angular resolution due to penetration is not a problem, we have found the experimental arrangement described in section 2.4 and Fig. 4 to be desirable. The absorption correction for this arrangement is not independent of scattering angle, but its form is easily derived²⁸. Fig. 16 shows the essential geometry, idealized for parallel beams, a satisfactory approximation to the divergent beam case²⁸. The scattered intensity is given by

$$I(\theta) = I_0 S \int_0^T W(\alpha \csc \theta - 2t \text{ctn} \theta) \exp(-2\mu t \csc \theta) dt$$

which, after integration, yields

$$I = (I_0 S W \alpha / 2\mu) [1 - (1 - \exp(-x))/x,]$$

where $x = 2\alpha \mu / \sin(2\theta)$, S the scattering cross section per unit volume of the

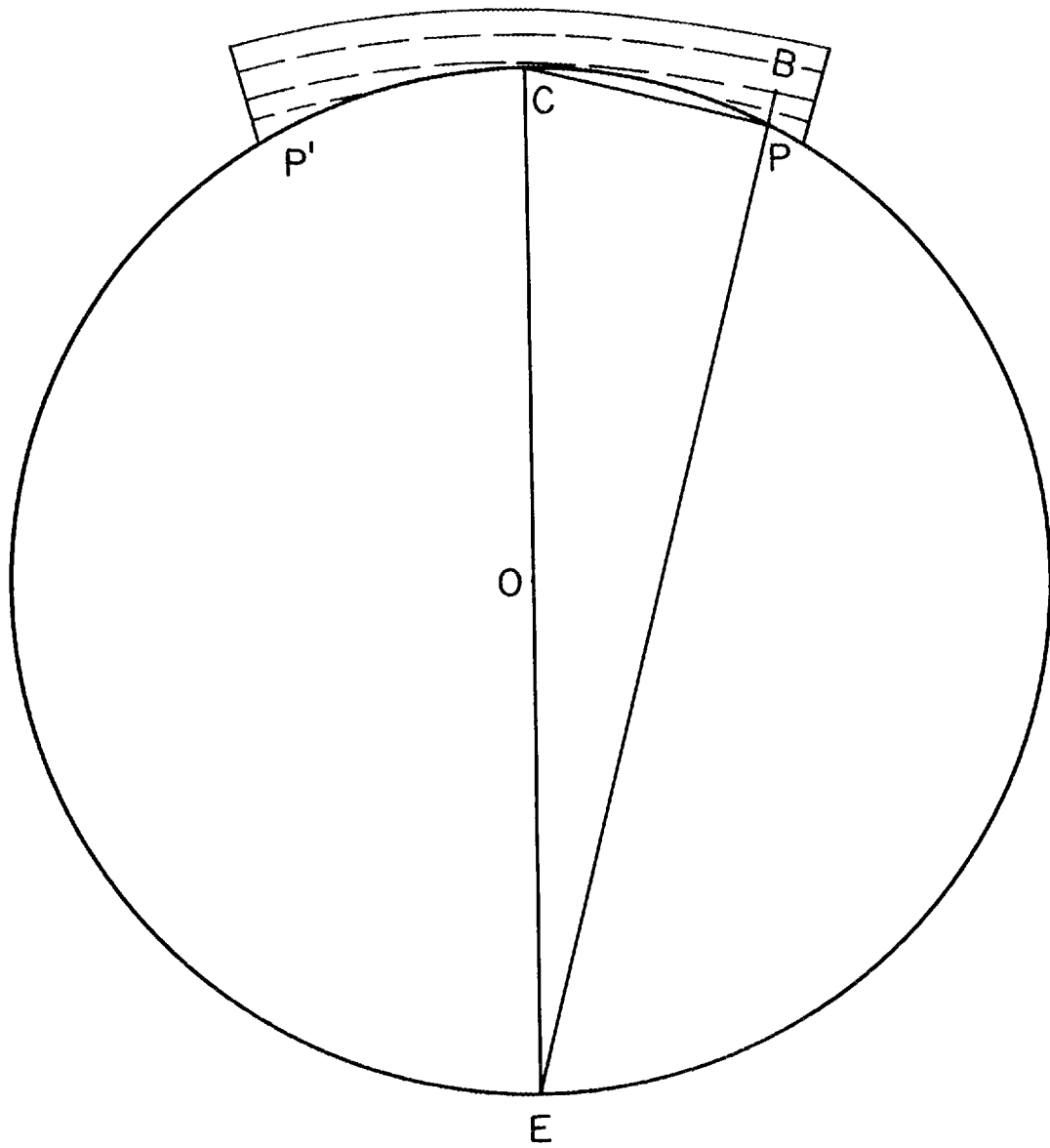


Fig. 17. Focussing Condition for Crystal Monochromator.

sample, and the other symbols are defined in section 8.1.1 and Fig. 16. It is seen that as μ , and hence x , becomes large, the correction factor (in brackets) approaches unity, the usual case.

8.2 Proof That Crystal Bent to a Radius and Ground to Half the Radius Satisfies the Bragg Focussing Condition

The circle in Fig. 17 represents the surface to which the crystal is ground after first being bent to radius EC (see section 2.3). Let line EB be the radius of the planes of the bent crystal passing through B and tangent to the final circle at C. EB is perpendicular to the crystal planes at B and is perpendicular to the planes at P on the reasonable assumption that the bending of the crystal maintains the crystal planes parallel. Thus the chord CP is tangent to the planes at P, since it is also perpendicular to the line EP. This will be true for any point P along arc P'CP, and thus all the crystal planes along this arc satisfy the Bragg focussing condition, namely, that crystal planes set along the arc with the planes parallel to the chord from each point drawn to C will focus the same wavelength from S_3 to D (Fig. 3).

9. REFERENCES

1. F. Zernicke and J. Prins, *Zeitschrift für Physik*, 41, 184 (1927); *ibid.*, 56, 617 (1929).
2. P. Debye and H. Menke, *Physikalische Zeitschrift*, 31, 797 (1930).
3. G. Fournet, *Handbuch der Physik*, Vol. XXXII, p. 239, Springer, Berlin, 1957.
4. R. F. Kruh, *Chem. Revs.*, 62, 319 (1962).
5. P. A. Agron, M. D. Danford, M. A. Bredig, H. A. Levy and P. C. Sharra, *Acta Cryst.*, 10, 739 (1957).

6. W. H. Bragg, Proc. Phys. Soc. London, 33, 222 (1921); J. C. M. Brentano, *ibid.*, 37, 184 (1925); Phil. Mag., 6, 178 (1928); Proc. Phys. Soc. London, 47, 932 (1935); *ibid.*, 49, 61 (1937).
7. J. W. DuMond and H. A. Kirkpatrick, Rev. Sci. Inst., 1, 88 (1930); T. Johansson, Zeitschrift für Physik, 82, 507 (1933); R. M. Bozarth and F. E. Haworth, Phys. Rev., 53, 538 (1938); J. W. DuMond, D. A. Lind and E. R. Cohen, Rev. Sci. Inst., 18, 617 (1947); J. W. DuMond, *ibid.*, 18, 626 (1947).
8. J. W. DuMond, D. A. Lind and E. R. Cohen, Rev. Sci. Inst., 18, 617 (1947).
9. L. S. Birks and E. J. Brooks, Rev. Sci. Inst., 24, 9922 (1953).
10. P. Debye, Annalen der Physik, 46, 809 (1915).
11. J. Waser and V. Schomaker, Rev. Mod. Phys., 25, 671 (1953).
12. A. H. Compton, Phys. Rev., 21, 715 (1923); *ibid.*, 22, 409 (1923).
13. J. Krogh-Moe, Acta Cryst., 9, 951 (1956); N. Norman, *ibid.*, 10, 370 (1957).
14. A. Rahman, J. Chem. Phys., 42, 3540 (1965).
15. H. S. Green, The Molecular Theory of Fluids, Interscience, New York, 1952.
16. H. S. Green, Handbuch der Physik, Vol. X, p. 47, Springer, Berlin, 1960.
17. M. Born and H. S. Green, Proc. Roy. Soc. A, 188, 10 (1946).
18. Reference 15, p. 75.
19. J. G. Kirkwood, J. Chem. Phys., 3, 300 (1935).
20. M. D. Johnson and N. H. March, Phys. Letters, 3, 313 (1963).
21. J. S. Rowlinson, Molecular Physics, 9, 197 (1965).
22. W. R. Busing and H. A. Levy, OR GLS, A General Fortran Least Squares Program, ORNL-TM-271 (August 1962).
23. M. D. Danford and H. A. Levy, J. Am. Chem. Soc., 84, 3965 (1962).
24. Y. Morino, Y. Nakamura and T. Iijima, J. Chem. Phys., 32, 643 (1960).

25. H. A. Levy and M. D. Danford, Diffraction Studies of the Structure of Molten Salts, Molten Salt Chemistry, M. Blander (ed.), Interscience, New York, 1964, p. 109.
26. H. A. Levy, P. A. Agron and M. D. Danford, J. Chem. Phys., 30, 1486 (1959);
ibid., 31, 1458 (1959).
27. A. Guinier, X-ray Diffraction, W. H. Freeman, San Francisco, 1963.
28. H. A. Levy, P. A. Agron and M. D. Danford, J. Appl. Phys., 30, 2012 (1959).

INTERNAL DISTRIBUTION

- | | |
|--------------------------------------|-----------------------------------|
| 1. Biology Library | 158. C. E. Larson |
| 2-4. Central Research Library | 159. H. A. Levy |
| 5. Reactor Division Library | 160. A. P. Litman |
| 6-7. ORNL - Y-12 Technical Library | 161. H. G. MacPherson |
| Document Reference Section | 162. A. H. Narten |
| 8-142. Laboratory Records Department | 163. D. R. Nelson |
| 143. Laboratory Records, ORNL R.C. | 164. A. S. Quist |
| 144. R. Baldock | 165. R. M. Rush |
| 145. H. Beutler | 166. D. R. Sears |
| 146. R. E. Biggers | 167. M. J. Skinner |
| 147. N. J. Bjerrum | 168. G. P. Smith |
| 148. C. R. Boston | 169. E. H. Taylor |
| 149. M. A. Bredig | 170. A. M. Weinberg |
| 150. W. R. Busing | 171. F. R. Winslow |
| 151. M. D. Danford | 172. H. L. Yakel |
| 152. H. A. Friedman | 173. J. P. Young |
| 153. R. W. Hendricks | 174. C. A. Hutchison (consultant) |
| 154. J. S. Johnson | 175. J. J. Katz (consultant) |
| 155. W. H. Jordan | 176. J. E. Meyer (consultant) |
| 156. H. W. Joy | 177. I. Perlman (consultant) |
| 157. B. H. Ketelle | 178. G. Scatchard (consultant) |

EXTERNAL DISTRIBUTION

179. J. A. Swartout, 270 Park Avenue, New York 17, New York
180. Research and Development Division, AEC, ORO
181-505. Given distribution as shown in TID-4500 under Chemistry category
(75 copies - CFSTI)